Slow hot-carrier cooling in halide perovskites : prospects for hot-carrier solar cells

Li, Mingjie; Fu, Jianhui; Xu, Qiang; Sum, Tze Chien

2019

Li, M., Fu, J., Xu, Q., & Sum, T. C. (2019). Slow hot-carrier cooling in halide perovskites : prospects for hot-carrier solar cells. Advanced Materials, 31(47), 1802486-. doi:10.1002/adma.201802486

DOI: 10.1002/ ((please add manuscript number))
Review

Slow Hot-Carrier Cooling in Halide Perovskites: Prospects for Hot-Carrier Solar Cells

*Mingjie Li, Jianhui Fu, Qiang Xu, and Tze Chien Sum**

Dr. M. Li, J. Fu, Dr. Q. Xu, Prof. T. C. Sum
Division of Physics and Applied Physics, School of Physical and Mathematical Sciences
Nanyang Technological University, 21 Nanyang Link, Singapore 637371, Singapore
E-mail: Tzechien@ntu.edu.sg

Keywords: Shockley-Queisser limit, hot carriers, halide perovskite, phonon bottleneck, hot-carrier solar cell

Rapid hot-carrier cooling is a major loss channel in solar cells. Thermodynamic calculations reveal a 66% solar conversion efficiency for single junction cells (under 1-sun illumination) if these hot-carriers are harvested before cooling to the lattice temperature. A reduced hot-carrier cooling rate for efficient extraction is a key enabler to this disruptive technology. Recently, halide perovskites emerge as promising candidates with favorable hot-carrier properties: slow hot-carrier cooling lifetimes several orders of magnitude longer than conventional solar cell absorbers; long-range hot-carrier transport (up to ~600 nm) and highly efficient hot-carrier extraction (up to ~83%). This review seeks to present the developmental milestones; distill the complex photophysical findings and highlight the challenges and opportunities in this emerging field. A developmental toolbox for engineering the slow hot-carrier cooling properties in halide perovskites and prospects for perovskite hot-carrier solar cells will also be discussed.

1. Introduction

The phenomenal rise in photovoltaic (PV) efficiencies of organic-inorganic halide perovskites heralded a new era of low-cost solution-processed photovoltaics with current record efficiencies surpassing 22%.[1-5] Recently, improvements to perovskite solar cells efficiencies have been extremely sluggish. To drive efficiencies towards their Shockley-Queisser (SQ)

limit and beyond, one unconventional approach to invigorate the field is to explore novel concepts like hot-carrier solar cell (HCSC). For all single junction solar cells, including perovskite solar cells, rapid cooling of hot-carriers (HCs) is a major energy loss process. Much higher solar cell efficiency is theoretically possible if such energy loss is mitigated. The basic idea behind HCSC is to extract these HCs before they lose their excess energy as heat. Thermodynamic calculations disclose that single-junction HCSC solar conversion efficiency can exceed the SQ limit (~33% for standard cell with band gap 1.4 eV) and reach around 66% under 1-sun illumination.[6] However, HC cooling typically occurs very rapidly (within hundreds of femtoseconds), making HCs extraction extremely challenging. A reduced HC cooling rate in solar absorbers is therefore a key material criterion for realizing HCSC.

Halide perovskites possess novel slow HC cooling properties favorable for development as HCSC. Since the first reports of slow HC cooling (~ 0.4 ps) in $MAPbI_3$ polycrystalline thin films,[7, 8] there have been growing interests about this novel phenomenon. Li *et al.* reported a drastic slowdown of HC cooling by a further 2 orders in $MAPbBr_3$ colloidal nanocrystals (~30 ps) and demonstrated efficient (~83%) extraction of HCs with an energy selective organic layer.[9] Long HC transport lengths (~600 nm) in $MAPbI_3$ thin films were visualized by Huang *et al.*[10] These exciting findings forebode the potential of perovskite HCSCs that could dramatically boost perovskite solar cell efficiencies beyond their SQ limits. Presently, the origins and mechanisms of slow HC cooling in halide perovskites remain fragmented and confusing with disparate models being proposed. A clear understanding of the intrinsic photophysics of HC cooling is essential for further technological developments.

In this review, we examine the milestones and advancements of slow HC cooling in halide perovskites and distill their photophysical mechanisms. We begin with a brief introduction of the operation principles of HCSCs and carrier relaxation processes, followed by highlighting

the seminal experimental and theoretical works on slow HC cooling in halide perovskites, before explicating their origins and mechanisms. A developmental toolbox for engineering slow HC cooling in halide perovskites and developing new perovskite materials with slower HC cooling will also be discussed. Lastly, we highlight the challenges and opportunities for perovskite HCSCs.

2. How hot carriers can be used?

We begin with a quick overview of the several concepts for high-efficiency solar cells. **Figure 1**a illustrates the energy band diagram of a typical single junction solar cell with its major energy loss processes following light illumination.[11, 12] In all solar cells, photons possessing energies greater than the semiconductor bandgap can create free carriers or excitons with excess energies above the bandgap. These carriers or excitons with a temperature higher than the lattice temperature are termed "hot carriers" or "hot excitons". These hot species then rapidly relax (within sub-picoseconds) to the band edge by losing their excess kinetic energies to phonons (or as heat) via electron-phonon scattering, before becoming available for transport to the contacts for charge extraction. This loss of energy to the phonons (*i.e.*, HC cooling) constitutes one of the major loss channels for PV efficiency, *e.g.*, ~ 25% in a single junction perovskite solar cell with bandgap 1.5eV (*i.e.*, corresponding to $MAPbI_3$) (Figure 1b).

Figure 1c shows a wide range of PV concepts capable of exceeding the conventional SQ limit through minimizing the above losses.[12, 13] Essentially, the concept of HCSC is based on the collection of "hot" carriers, arising from the absorption of the wide range of photon energies, to the external circuit whilst they remain hot, thereby increasing the voltage of the cell.[11, 14] Extending the original SQ detailed balance approach to HCSC, Figure 1c shows the thermodynamic solar conversion efficiency for an ideal single-junction HCSC (*i.e.*, assuming no loss of excess energies above threshold) to be as high as ~67%,[6] which is approaching the

efficiency limit of an infinite tandem cell under 1-sun irradiation (Figure 1d, green lines). To stretch the HCSC limits even further, concentrated solar irradiation can also be applied.[15] For instance, the efficiency can reach as high as ~75% under a concentration of 100 Suns irradiation for 3000K-HCs (Figure 1d, orange lines).

A related approach that leverages slow HC cooling for efficient energy extraction of HCs is multiple exciton generation (MEG). MEG or carrier multiplication (CM) is a process that generates more than one electron-hole pair from the absorption of one high-energy photon (with at least twice the bandgap energy, E_g), which can boost the photovoltaic efficiencies to ~44% - Figure 1c.[16-18] Perovskite NCs with their novel slow hot-carrier cooling [9] are therefore also highly promising candidates for MEG. Indeed, Li *et al.* most recently demonstrated efficient MEG (up to ~75% in slope efficiency) with low MEG thresholds (down to ~2.25E_g) in intermediate-confined colloidal formamidinium lead iodide nanocrystals [19] – aptly highlighting their potential for MEG solar cells. The abovementioned tandem cell (or multi-junction cell) tackles the HC energy loss problem in a slightly different approach.[20,21] In these cells, multiple absorber materials with different band gaps are stacked sequentially to absorb different wavelength regions of the solar spectrum; and connected via tunnel junction layers for charge extraction. Effectively, this approach can help mitigate the HC energy loss problem in a single bandgap absorber by extending the absorbance to a wider range of wavelengths with multiple sub-cells – thereby exceeding the single-junction efficiency limit. Nonetheless, tandem cells are both highly complex and costly, requiring meticulous and challenging fabrication. Here, our review focuses primarily on HCSC.

Although HCSCs offer such attractive high efficiencies (Figure 1c), a major hurdle to realizing practical devices is the fast cooling of HCs in the absorber material. Conventional semiconductor materials (such as GaAs[22], InN[23] etc, see **Table 1**) suitable for HC absorbers

are few and far between. Attempts to leverage the hot phonon bottleneck effect observed in InN for photovoltaics have been unsuccessful due to various reasons such as challenging fabrication process, poor material quality and low abundance of In, *etc.*[24, 25] This traditional hurdle can now be transcended with halide perovskites.[22, 26-31] We shall next review the dynamics of HC cooling in semiconductors, followed by a discussion on the findings of slow HC cooling dynamics in halide perovskites; and subsequently a review of its origins and mechanisms.

3. Typical HC Cooling Dynamics

Figure 2 shows the basic photophysical processes of HC cooling in semiconductors and a schematic evolution of the electron and hole distributions with time following above bandgap pulsed laser excitation.[14] After absorbing the high energy photons (Process 1), the HCs will redistribute the energy and relax via various pathways to reach thermal equilibrium with the lattice. The energetic carriers will first thermalize among themselves through carrier-carrier interactions and intervalley scattering. This process occurs very rapidly (within 100 fs) and is usually called carrier thermalization (Process 2), which eventually result in the HCs fulfilling the Boltzmann statistics with a carrier temperature T_c that is larger than the lattice temperature T_L. The HC thermalization process in halide perovskite shows some similarities. Direct observation of ultrafast carrier thermalization in perovskites was first reported by Richer, et al using two-dimensional electronic spectroscopy with a characteristic thermalization time from 10 fs to 85 fs.[28]

Following carrier thermalization, the thermalized HCs will start to equilibrate with the lattice mainly through inelastic carrier-phonon interactions. The next stage is known as “cooling” of HCs, which comprises of processes 3-5. However, the term thermalization has often been erroneously ascribed to this process, which causes confusion with the earlier stage of equilibration. To make matters worse, the term “thermalization loss” is often used by the PV

community to refer to the loss of the HC's excess energy as heat. Here, we follow the definition set by the ultrafast community and distinguish that the earlier stage of carrier relaxation (immediately following photoexcitation) refers to carrier thermalization while the subsequent process as carrier cooling.

Generally, HC cooling via electron-LO-phonon scattering (process 3) occurs within 1ps. Due to the polar nature of the perovskites, the dominant relaxation pathway for the HCs in perovskites is through Fröhlich interactions, *i.e.*, electron-LO-phonon scattering. Notably, polarons can also be formed during process 3, due to the large electron-phonon interactions coupled with lattice deformations.[32] A polaron is formed through the interactions between a charge carrier and its surrounding lattice, where the carrier and surrounding polarization then behaves collectively like a quasi-particle. The electron-LO-phonon scattering process continues till the excess energies of the HCs is less than the LO phonon energy. Then, the emitted LO phonons from electron-LO-phonon scattering can decay into the daughter acoustic phonons and/or transverse optical phonons (Process 4). Following which, the energy will be lost via decay of acoustic phonon emissions, which usually occurs in hundreds of picoseconds (Process 5). Lastly, the cooled carriers will recombine (usually in nanosecond timescale - Process 6). In the case of continuous optical pumping, an equilibrium state of the system is reached when the energy absorbing rate by the HCs from the laser is balanced with the energy loss rate from various equilibration pathways. Next, we trace the milestones of slow HC cooling phenomena in halide perovskites.

4. Observations of Slow HC Cooling in Perovskites

Slow HC cooling in halide perovskites was first reported in 2013 by Xing *et al.* using transient absorption (TA) spectroscopy to probe the higher-energy photobleaching (PB) band (PB1 at ~480 nm) in $MAPbI_3$ polycrystalline films (**Figure 3**a-c).[8] The slow rise of the band-

edge bleach signal together with a concurrent decay of a deeper level bleach signal both with lifetimes of ~0.4 ps under pump energy (3.1 eV) is attributed to slow hole cooling (Figure 3c, left panel). This 0.4-ps HC cooling time is slower than most organic semiconductors (~100 fs),[33, 34] and originates from the hot-hole relaxation from a deeper valence band state VB1 to the band edge VB2 states (Figure 3b). A follow-on work by Sum's group later reported similar concomitant rise and decay bleach signals for the conduction band states CB1 and CB2 as well.[7] This indicates that the slow hot-electron cooling process (*i.e.*, from CB1 to band edge CB2 state in Figure 3b) also occurs at ~0.4 ps (Figure 3c, right panel). Readers interested in the interpretation of these states and dynamics can refer to the following references.[7, 8, 35] The findings that both the hot holes and hot electrons cooling lifetimes are relatively balanced in halide perovskites has important ramifications for the development of practical HC optoelectronics. The HC cooling rates are pump fluence dependent as validated by Chen *et al.*, who reported even slower HC cooling up to ~10 ps in $MAPbI_{3-x}Cl_x$ films – evident from the substantially prolonged high-energy tail (Figure 3d), and delayed build-up of the ground state bleaching signals with increasing pump fluence to 340 μJ cm^{-2} (Figure 3e).[36] These fascinating slow HC cooling phenomena intrigued researchers and triggered a slew of experimental and theoretical studies to understand its origins and mechanisms; as well as potential applications in low-cost HCSCs.[22, 28-31, 37-45] These studies include the dependence of photoexcited carrier density[9, 22, 30, 46-48], the initial HC excess energy[22, 46, 47], cation species[30, 31, 46, 49], morphology[50] and confinement effects (in nanocrystals)[9, 51] on the HC cooling dynamics.

Table 1 shows a comparison of the HC cooling times for halide perovskites and other conventional semiconductors. It must be noted that HC cooling rates are dependent on the photoexcited carrier density, the initial HC excess energy, as well as the resolution of the instrument used. Hence, due care must be taken when making a reasonable comparison

between reports from different groups. For sake of clear and easy comparison of HC cooling lifetimes (or rates) reported for different semiconductors in the literature, the HC cooling time from the initial temperate and cooled to 600 K is listed for comparison. 600K is used as the benchmark as previous calculations have shown that extraction of HCs with T_c > 600 K, an appreciable HC conversion efficiency (*i.e.*, > 40%, see Figure 1d) over a wide range of absorber bandgaps is still present.[6] Various mechanisms including hot-phonon bottleneck, acoustic-optical phonon upconversion, Auger-heating, band-filling, large polaron formation, and intrinsic phonon bottleneck effects have also been proposed, which will be discussed in detail in the following section.

5. Mechanisms Behind Slow HC Cooling

5.1 Hot-Phonon Bottleneck Effect

The LO hot-phonon bottleneck effect is widely used to account for the slow HC cooling effect in polar semiconductors.[58-60] This bottleneck effect usually occurs in highly excited semiconductors and has recently been observed in perovskites in the presence of a non-equilibrium LO-phonon population that leads to reduced net LO-phonon emission and re-heating of carriers, thus slowing the HC cooling.[22,28,29] The HC cooling phenomena is a cascade process between carrier-LO-phonon scattering and LO-phonon decay. The presence of hot-phonon effect is determined by the competition between the phonon decay rate and the carrier-density dependent carrier-LO-phonon scattering rate.[61]

The HC temperature can be obtained by fitting the high-energy tail of band-edge photobleaching TA spectrum using the Maxwell–Boltzmann distribution function (**Figure 4**a redlines): [22, 62-64]:

$$\Delta A(E) = -A_0(E)\exp(-\frac{E}{k_B T_c}) \quad (1)$$

where ΔA the transient absorbance, T_e is the HC temperature, k_B the Boltzmann constant. Since ΔA proportional to the summation of the contribution from both the electron and the hole, the carrier temperature is thus the average temperature between the electron and the hole. The TA technique monitors the occupancy of the states (*i.e.*, regardless of radiative and non-radiative processes) unlike the hot-PL approach undertaken in some reports[43], [65] (discussed later), which is only sensitive to the emissive species. One limitation of the TA technique is its inability to simply discern the respective contributions of the electron and hole; unlike the two-photon photoemission which directly probes the dynamics of hot electrons above the Fermi level.[66] Nonetheless, given their similar effective masses (m_e = 0.19m_0, m_h = 0.25m_0),[67] comparable contributions from hot electrons and hot holes to the extracted HC temperatures are expected. In the absence of the hot-phonon effect, the HC cooling dynamics can be modeled using the Fröhlich interaction model with the energy loss rate[22, 62-64] of the HCs as follows:

$$\frac{dU_c}{dt} = \frac{3k_B}{2}\frac{dT_e}{dt} \approx -\frac{\hbar\omega_{LO}}{\tau_{ave}}\left[\exp(-\frac{\hbar\omega_{LO}}{k_B T_e}) - \exp(-\frac{\hbar\omega_{LO}}{k_B T_c})\right] \quad (2)$$

where $\hbar\omega_{LO}$ the LO-phonon energy, τ_{ave} the average HC cooling time, T_L is the lattice temperature. As reported by Y. Yang *et al.*, the HC cooling dynamics in $MAPbI_3$ film at low pump fluence (<10^{18} cm^{-3}) can be well described using Equation (2) with lifetime <1 ps with higher initial T_e at higher carrier densities and excess energies (Figure 4b).[22] At high pump fluence (>10^{18} cm^{-3}), carrier cooling dynamics deviates from the calculated curves based on above equation (Figure 4c), indicating the presence of hot-phonon effect. The lifetime of HC temperature cooling to 600K increase dramatically to ~60 ps, almost 2 orders of magnitude larger than that at low pump fluence. Such hot-phonon bottleneck is also observed $FAPbI_3$ film (Figure 4d).[22, 29] Impressively, the HC cooling time at high pump fluence in hybrid perovskites can be ~100 times longer than that in GaAs film[22] and CdS microplates[54] (Table

1). The authors attributed the stronger hot-phonon bottleneck effect in hybrid perovskite to the larger electron–phonon interaction than conventional semiconductor, which leads to a more rapid build-up of a hot LO-phonon population and slower rate of conversion of LO-phonons to acoustic phonons.

J. Yang *et al.* also investigated the influence of the organic cation and halide cation on the carrier cooling dynamics using TA spectroscopy combined with phononic density functional theory (DFT) calculations.[30] An approximately 10 times longer LO-phonon emission lifetime was observed in highly excited $FAPbI_3$ films than their all inorganic counterparts with the same 3.1eV photoexcitation energy (Figure 4e). They attributed the hot-phonon effect to originate from acoustic-optical phonon upconversion, where the overlapping phonon branches by organic cations enhanced the up-transition of low-energy phonon modes. The efficient acoustic phonon up-conversion can thus reheat carriers via recycled thermal energy. The authors argued that the slower HC cooling in $FAPbI_3$ is due to better phonon band overlap and stronger acoustic phonon localization as well as the lower thermal conductivity. However, this acoustic-optical phonon up-conversion mechanism is primarily based on the findings of another work[68] for a (thermally) insulating layered (two-dimensional (2D)) perovskite system $(C_6H_5CH_2CH_2NH_3)_2CuCl_4$). Thus, the underlying assumption is that 3D and 2D halide perovskites possess similar thermal properties. This need not be the case as reported in another publication on laser cooling of 2D and 3D halide perovskites,[69] the measured maximum thermal cooling for a 2D perovskite system is about 300 Km W^{-1} while that for a 3D perovskite is about 35 Km W^{-1} (*i.e.*, 1 order difference between 3D and 2D halide perovskites). Further investigations are warranted.

A rigorous consideration of HC cooling dynamics in 3D perovskite was later undertaken by Fu *et al.*[29], who accounted for the interplay between electron-LO-phonon scattering and LO-

phonon decay (Figure 4f). Our results revealed that from moderate carrier concentrations (~10^{18} cm^{-3}), polar Fröhlich electron-phonon interactions mediate the carrier cooling via zone-center delayed LO-phonon emissions that are induced by the hot-phonon bottleneck. The obtained ~0.6 ps LO-phonon lifetime is much longer than that of the typical ~10 fs electron-LO-phonon scattering time without the hot-phonon bottleneck effect. This is due to the suppression of the essential Klemens relaxation channel for LO-phonons (*i.e.*, LO $\rightarrow$ 2LA phonons) by the larger phononic bandgap ($E_{LO\text{-}min}$-$E_{LA\text{-}max}$) than the maximum acoustic phonon energy in $MAPbI_3$.

5.2 Auger Heating Effect

At higher HC densities (~10^{19} cm^{-3}), apart from the hot-phonon bottleneck effect, the multi-particle Auger-heating effect can further retard the HC cooling to several hundreds of picoseconds in hybrid perovskites films (Figure 4f).[28, 29] The non-radiative Auger-heating process involves the transfer of the electron-hole recombination energy to another carrier that leads to excitation of this carrier to an even higher energetic state (inset of Figure 4f).[70] The recombination energy transferred to the electronic system is proportional to $E_g + E$, where E_g the bandgap.[71] The carrier cooling dynamics including the Auger-heating effect can be described by the following expression:

$$\left\langle \frac{dE}{dt} \right\rangle_{tot} = \left\langle \frac{dE}{dt} \right\rangle_{e\text{-}ph} + k_3 n^2 (E_g + E) \quad (3)$$

$$\frac{dn}{dt} = -k_1 n - k_2 n^2 - k_3 n^3 \quad (4)$$

where k_1 the monomolecular recombination coefficient, k_2 is the free carrier bimolecular recombination coefficient, and k_3 the Auger recombination coefficient, which is larger for smaller bandgap and higher carrier temperature.[70] The first term on the right side of Equation (3) refers to the energy loss rate via electron-LO-phonon interaction, while the second term

corresponds to the Auger-heating contribution. The strong Auger-heating effect on HC cooling in lead iodide perovskites is attributed to its relatively small bandgap and the significant hot-phonon effect.[29] On the other hand, the Auger-heating effect will be even more dominant in perovskite nanostructures. This is due to the momentum conservation and greater overlap of the carrier wavefunctions under quantum confinement (which is indeed present in many semiconductor nanostructures such as GaAs/AlAs multiple quantum wells and CdSe quantum rods).[70, 73] Nonetheless, for developing practical HC optoelectronics, one needs to carefully consider the carrier depopulation arising from the Auger effect even though HC cooling lifetimes can be further retarded.

5.3 Large Polaron Formation at Low Carrier Density

An exciting addendum to the abovementioned typical mechanisms of slow HC cooling in halide perovskites is the large polaron picture (*i.e.*, polarons whose size of the polarization cloud is ~10× unit cell dimension). Zhu *et al.* proposed that this mechanism is distinct from the hot phonon bottleneck effect, occurring at low carrier density ($<10^{18}$ cm^3). Zhu *et al.* reported long-lived HC photoluminescence (with ~150 ps lifetime scale) from HCs (with initial electronic temperature of ~580K) in $MAPbBr_3$ and $FaPbBr_3$ single-crystals (under 3.06 eV-photoexcitation at low carrier densities $\leq 10^{17}$ cm^{-3}) with the time-correlated single photon counting (TCSPC) technique (instrument response function ~90 ps).[31] In contrast, such long-lived hot-PL emission was not observed in all inorganic $CsPbBr_3$ counterpart. **Figure 5**a shows the room-temperature pseudo color TRPL plot of $MAPbBr_3$, which has a strong band-edge emission along with a high-energy tail expanding up to ~300 meV above the band-edge. The HC temperature T^* was extracted by global fitting of the transient PL spectra (Figure 5b) (based on a model of two thermalized band-edges and hot carrier populations), which decrease from 1250 ± 200 K with a cooling lifetime of 150 ± 30 ps, that eventually approach

the asymptotic value of T_{as} = 670 ± 100 K (Figure 5c). It should be noted that T_{as} is higher than the equilibrium sample temperature of 293 K due to the intrinsic PL spectra broadening.[74] Thus, the actual initial HC temperature should be ~580 K.

The scattering of charge carriers with LO-phonons, charge defects and even with one another can be reduced by the dynamic screening in polar semiconductors. Such dynamic screening has been proposed to account for the remarkable transport properties of halide perovskites.[74, 77-79] Zhu *et al.* proposed that the dynamical screening from the reorientational motions of the dipolar molecular cations and the large polaron formation give rise to the long-lived HCs in organic-inorganic hybrid perovskites.[10, 80, 81] From time-resolved optical Kerr effect (TR-OKE) measurements, they proposed a polaron formation time of ~0.3 ps in $MAPbBr_3$ and 0.7 ps in $CsPbBr_3$, respectively (Figure 5d).[10] They suggested that the large polaron formation rate competes favorably with the initial LO-phonon cooling time to greatly slow down the HC cooling in $MAPbBr_3$. Large polaron formation was also correlated with the charge carrier transport properties, particularly the inverse temperature dependence in charge carrier mobilities,[82, 83] and ~1.5 times lower thermal conductivity of $MAPbI_3$ compared to $CsPbI_3$, and also 1-2 orders lower than those in typical semiconductors.[84-86] This purported phonon glass character and slow acoustic phonon transport may contribute to the slow cooling of HCs. The authors argued that the absence of long-lived hot-PL emission from the low-temperature orthorhombic phase of $MAPbBr_3$ was due to the freezing of the liquid-like motions of MA ions.[31]

Another striking observation by Zhu *et al.* is that the high-energy tail of the initial PL spectra reduces with increasing pump fluence as shown in Figure 5e for $MAPbI_3$ film. Their results show that HC temperature reduces with increasing carrier densities (up to 2×10^{18} cm^{-3} - Figure 5f). These results contrast with the opposite trend widely reported for $MAPbI_3$ films (obtained

from TA measurements over similar carrier densities) with much higher HC temperatures that are attributed to the hot-phonon bottleneck effect (Figure 4)). The authors argued that HC cooling rate becomes faster because of the destabilization of the large polarons caused by greater inter-polaron repulsive interaction, which increasingly weakens the protective large polaron shield (with higher excitation densities) until the onset of hot-phonon bottleneck (at pump fluence $\geq 10^{18}$ cm^{-3}). Effective mass theories combined with first-principles calculations by Frost *et al.* show that the critical Mott density where large polarons begin to spatially overlap is approximately 10^{18} cm^{-3}, lending crucial theoretical support to this interpretation.[87] Further studies are warranted to rationalize the contrasting trends for the HC temperatures and to better understand the transition of HC cooling from the large polaron protection model at very low carrier densities (~10^{16} cm^{-3}) to the hot-phonon bottleneck effect at high carrier densities ($\geq 10^{18}$ cm^{-3}).

5.4 Band-filling at High Carrier Density

Even longer lived HC emissions (with ns lifetimes) from streak camera TRPL measurements were recently reported for $FASnI_3$ thin films at high carrier densities (>10^{18} cm^{-3}).[43] **Figure 6**a shows the pseudo-color TRPL spectra of $FASnI_3$ thin films under 3.1 eV photoexcitation at room temperature. With increasing pump intensity, the emission peak shifts towards high energy (up to 75 meV and follows the $n^{2/3}$ law with carrier density n), together with an increased contribution of higher energy hot-PL (Figure 6b). Such long-lived HCs with few-ns lifetimes and a large blue shift of the band-edge emission energy was attributed to the band-filling effect (Figure 6c).[88] Interestingly, the obvious blue-shift of emission energy is absent from lead halide perovskites ($MAPbI_3$ or $FAPbI_3$) films under similar excitation conditions. The high pump fluence used also contrasts with the polaron protection model (which is a low pump fluence effect). Slow HC emission becomes more obvious at higher excitation intensity and is observed at a low temperature of 24 K. The authors speculated that the reasons for such

blue-shift of PL and long-lived hot PL in $FASnI_3$ could originate from the Rashba effect and/or from the chemical pressure on the inorganic lattice that resulted in the shallow defects in $FASnI_3$ becoming deeper. Notably, the large energy blue shift and high-energy tail are also present in steady-state PL spectra of $FASnI_3$ film under high pump-fluence continuous-wave excitation (Figure 6d). Accordingly, the extracted initial HC temperature and HC population at 44 suns contribute to ~500K and 60%, respectively (Figure 6e). Such strong emission from HCs under continuous-wave (CW) operation is an important development towards realizing HCSCs. Nonetheless, the long ns lifetimes of these hot-PL emissions should not be mistakenly interpreted as implications of higher potential for application in HCSCs. The HCs need to be rapidly harvested while remaining at their highest possible temperatures for maximal efficiencies (Figure 1d).

5.5 Intrinsic Phonon Bottleneck in Perovskite Nanocrystals

During the early years of nanoscience research, the intrinsic phonon bottleneck effect arising from energy and momentum conservation and large energy level spacing in quantum-confined systems was expected to yield reduced carrier-phonon coupling and HC cooling rates.[89-91] However, to date, achieving slow HC cooling in strongly quantum-confined conventional II-VI and IV-VI semiconducting NCs remains elusive. Further investigations revealed that other rapid relaxation pathways for HCs such as Auger-type energy transfer from the hot electrons to the dense hole states (**Figure 7**a)[92, 93], atomic fluctuations and defects trapping[94, 95] overcome this phonon bottleneck, resulting in a faster cooling rate as dimensionality decreases for nanoscale inorganic semiconductors.

Realizing the unique features of symmetric energy dispersion together with similar and small electron and hole effective masses for halide perovskites[96, 97] as compared to II-VI semiconductors, Sum's group emulated the nanoscale confinement approach to further retard

the hot carrier cooling using 3D perovskite NCs[9]. Unlike quantum-confined conventional II-VI semiconductors, the hole manifold is absent in perovskite NCs (Figure 7a), which will help sustain the intrinsic phonon bottleneck. Furthermore, the high PL quantum yield of 3D perovskite NCs (>80%) also means that the defect densities are low, thereby mitigating hot carrier losses. Slower HC cooling compared to their bulk perovskite counterparts and conventional semiconductor NCs, and intrinsic phonon bottleneck effect can indeed be achieved using weakly-confined colloidal $MAPbBr_3$ NCs (average radius around 2.5–5.6 nm). Figure 7b shows the obvious high energy tails in the photobleaching (PB) band that were fitted using the Fermi-Dirac distribution. Their extracted HC temperatures are much higher and HCs decay slower than the $MAPbBr_3$ bulk-film and other semiconductors under comparable photoexcitation conditions (Figure 7c and Table 1).

Apart from fitting the high energy tail of the PB peak, an alternative method to assess the HC cooling properties is to monitor the PB rise time of the bandedge carriers. This latter approach was commonly used for investigating the HC dynamics at low excitation densities in strongly confined quantum colloidal semiconductor NCs,[98, 99] due to the overlapping PB bands from the discrete energy levels, which makes resolving their HC distribution extremely challenging. The longer rise-time corresponds to a longer HC lifetime. This latter approach is useful for a fair comparison of the HC cooling of perovskites NCs with strongly quantum confined conventional inorganic semiconductor NCs. Figure 7d shows the size-dependent HC cooling lifetimes of $MAPbBr_3$ NCs compared to $MAPbBr_3$ bulk films and CdSe NCs (various sizes) at low pump fluence of $\langle N_0 \rangle$ ~0.1. Importantly, the trend for perovskite NCs rise times is converse of the CdSe NCs' trend. This result is a clear validation that the intrinsic phonon bottleneck effect remains intact in perovskite NCs. Our observation of the intrinsic phonon bottleneck effect also shows that the abovementioned competing processes (*i.e.*, Auger-type energy transfer, atomic fluctuations and defects trapping that plagues CdSe NCs) can be

effectively suppressed using perovskites NCs.

With increasing pump fluence (<N_0> ~2.5), the HC lifetimes in the perovskites NCs with more than one e-h pair (corresponding to effective volume carrier density of ~10^{18} cm^{-3}) become greatly retarded, reaching ~32 ps (Figure 7c). This is approximately 1-2 orders longer than its bulk-film counterpart under similar photoexcitation conditions (Table 1). We attribute this long HC cooling to originate from the Auger-heating effect. This is also consistent with our observations in perovskite films (albeit having a reduced effect (Figure 4f)). Considering that the Auger process is strongly enhanced in NCs due to the increased overlap of the carrier wave functions and interactions at higher carrier densities,[100] the relaxed HCs (at the band edges) can thus be efficiently re-excited to higher energy levels via Auger recombination (Figure 7a, right).

Similarly, long-lived HCs in weakly confined colloidal $FAPbI_3$ NCs (from the pump-induced lengthening of the TA band-edge bleaching rise-time) was also reported by P. Papagiorgis *et al.*[57] (Figure 7e-f). They observed three distinct HC cooling characteristics with lifetimes of sub-picoseconds, ~5 ps, and ~40 ps, that were attributed to carrier-LO-phonon scattering, hot-phonon bottleneck, and Auger-heating effect, respectively (Figure 7f). These observations clearly demonstrate the much slower HC cooling time in perovskite NCs at both low and high pump intensities, thus highlighting perovskite NCs as very promising candidates for HCSCs.

5.6 Toolbox for Engineering Slow HC Cooling in Halide Perovskites

Based on the insights gained from the various findings on slow HC cooling in halide perovskites together with the vast literature on HC cooling in traditional semiconductors,[18, 19] we attempt to assemble a rudimentary developmental toolbox for engineering slow HC cooling and designing even more efficient HC absorbers:

(1) *Enlarged Phononic Bandgap*: The phononic bandgap ($\hbar\omega_{\text{LO-min}} - \hbar\omega_{\text{LA-max}}$) must be much larger than the maximum $\hbar\omega_{\text{LA}}$ ($\hbar\omega_{\text{LA-max}}$) energy (*i.e.*, $\hbar\omega_{\text{LO-min}} - \hbar\omega_{\text{LA-max}} > \hbar\omega_{\text{LA-max}}$) in order to efficiently impede the Klemens channel for LO phonon decay. Consequently, this leads to the formation of a non-equilibrium phonon population and an LO hot-phonon bottleneck ensues. $MAPbI_3$ has a phononic bandgap energy/$\hbar\omega_{\text{LA-max}}$ ratio of ~ 2.2 (obtained from DFT calculated phonon spectra in **Figure 8**a), which is larger than ~1.7 for the well-studied InN HC absorber. A large atomic mass difference between the positively and negatively charged ions can lead to larger phononic bandgap and smaller h $\omega_{\text{LA-max}}$.[25] This can possibly be achieved through partial substitution of lead with heavier Bi^{3+} or lanthanides (such as Eu^{2+}, Tm^{2+}, and Yb^{2+}),[101] and/or partial substitution of I^- with lighter Br^- or Cl^-

(2) *Lower Thermal Conductivity:* Acoustic phonon up-transition is expected to be enhanced in perovskites by stronger localization of acoustic phonons and by blocking their propagation with lower thermal conductivities perovskites.[30] A low thermal conductivity (~0.5 W K^{-1} m^{-1}) for $MAPbI_3$ was reported.[84] Thus, α-$FAPbI_3$ or Ruddlesden-popper perovskites with even lower thermal conductivities[68], [102, 103] should also be considered.

(3) *Small LO Phonon Energy*: In the absence of the hot phonon effect, the energy loss rate of HC via carrier-LO phonon interaction can be expressed as:[29]

$$P_0 = \frac{m^{1/2}e^2}{\pi\varepsilon_0\hbar^2}\left(\frac{\hbar\omega_{\text{LO}}}{2}\right)^{3/2}\left[\frac{1}{\varepsilon_{\text{Opt}}} - \frac{1}{\varepsilon_{\text{Stat}}}\right] \quad (5)$$

where ε_{Opt} and ε_{Stat} are the optical and static dielectric constants. Smaller $\hbar\omega_{LO}$ requires more phonons for a given energy loss of HCs, which will slow down HC cooling. As shown in Figure 8b, $\hbar\omega_{LO}$ of both 3D and 2D perovskites are much smaller than conventional semiconductors. The small $\hbar\omega_{LO}$ (~ 8 meV) for $MAPbI_3$ arises from the low-frequency Pb-I stretching vibration because of the heavy lead. To further reduce $\hbar\omega_{LO}$, substitution of lead using heavier element (*e.g.*, $Cs_3Bi_2I_9$ and $MA_3Bi_2I_9$) may help obtain smaller $\hbar\omega_{LO}$ and thus slower HC cooling.

(4) *Smaller Carrier Effective Mass*: Based on equation 5 above, a lighter carrier effective mass will also lead to less efficient HC relaxation as shown in our calculated HC cooling dynamics for different carrier effective masses (Figure 8c). This is consistent with recent DFT findings of a small DOS at the valence bands of 3D perovskites result in a reduction of the available relaxation pathways as well as small effective mass.[37] Thus, computation screening of new perovskites (*e.g.*, double perovskites, Ruddlesden-popper perovskites *etc.*) for small effective mass is a possible criterion for designing HC perovskite absorbers.

(5) *Energetic Molecular Cations*: Based on the large polaron model,[31] HCs in hybrid perovskites are believed to be protected by large polarons arising from the fast molecular-reorientation motion that screen carrier-LO phonons interactions at low pump fluence. Thus, using organic molecular with smaller activation barrier energy for rotational motion (*e.g.*, FA^+ in α-$FAPbI_3$[104]) in halide perovskites could enhance the screening. Conversely, co-doping with Cs^+ could be an approach for regulating the size of the large polarons.

(6) *Multi-dimensional 2D/3D Ruddlesden-popper Perovskites*: The internal organic barriers can prevent or reduce diffusion of HCs and phonon confinement, thus maintaining non-equilibrium phonon populations. Furthermore, Ruddlesden–Popper perovskite quantum wells also have low thermal conductivity, internal self-charge carrier separation, and reduced charge recombination rate,[105] which will be beneficial for slow HC cooling and device operation. Modulation of the HC cooling dynamics can be achieved through tuning the organic cations (*e.g.*, PEA^+ = phenethylammonium, BA^+ = benzylammonium and $CHMA^+$ = cyclohexylammonium) between the inorganic lattices to vary the dielectric constants, carrier-carrier and carrier-phonon interactions *etc*.

(7) *Sample Morphology*: Sample morphological control is another possible approach to tune HC cooling.[106] Nah *et al.*[107] recently observed the higher initial HC temperature and slower HC cooling in smaller crystal domains in the polycrystalline $MAPbI_3$ film using spatial-resolved TA spectroscopy (~200 nm resolution).[107] Thus inhibition of crystal growth during fabrication (*e.g.*, adding MAI during $MAPbI_3$ film fabrication[108]) or usage of solvent additives to alter the carrier-carrier and carrier-phonon interactions are also feasible.

(8) *Perovskite Nanostructures and Quantum Confinement:* Perovskites nanostructures (*e.g.*, nanocrystals (NCs), nanowires (NWs), nanorods, nano-ribbons, and nanoplatelets *etc.*) are candidates to exploit the confinement effects on the carriers, excitons and phonons. For instance, perovskite NCs with better suppression of HC trapping by defects (e.g., benzoyl or benzyl-treated perovskites NCs with higher PL quantum yields[109, 110] or core/shell NCs[111]) will result in slower HC cooling as a result of the intrinsic phonon bottleneck especially at low pump fluence. Previously, long-lived HCs in III-V semiconductor NWs were observed for continuous wave (CW) excitation at high pump fluence.[112] It was found that higher temperature HCs were obtained from smaller diameter NWs (from hundreds to tens of nm) – induced by a suppression of available phonon modes due to the enhanced surface boundary scattering with smaller diameters. Similar behavior can be expected for perovskite NWs. Lastly, carrier confinement could also be used to enhance the Auger-recombination coefficients in halide perovskites, which can result in the slower HC cooling in NCs via Auger-heating at high pump fluence.[9]

6. HC Transport and Extraction

The long HC relaxation lifetimes in perovskites are expected to yield long HC travel distances. Direct observations of the HCs transport lengths, as well as the feasibility of extracting them from the absorber, provide important validations of their potential for realizing practical HCSCs. The following works aptly highlight the developments in this emerging area.

6.1 Long-range HC Transport

Direct observations of long-range HCs transport was first demonstrated by Huang *et al.*[42] using TA microscopy (TAM)[113-115] to simultaneously resolve the carrier dynamics

temporally and spatially at the photoinduced absorption (PIA) band at 1.58 eV (that is attributed to HCs[116, 117]). Three distinct carrier transport regimes, specifically, quasi-ballistic transport (~230 nm) for the initial HCs within ~300 fs, nonequilibrium transport (~600 nm) for the protected long-lived HCs over tens of ps, and diffusive transport for the cooled carriers were discerned at low carrier density of ~4×10^{17} cm^{-3}. **Figure 9**a shows the TAM images of ΔT_{PIA} intensity mapping at variant pump-probe delay time probed at 1.58 eV, from which the photoexcited carrier distribution n(x, y, t) was obtained by $\Delta T_{PIA}(x, y, t)^2$. At 0 ps after 3.14eV pump (corresponding to HCs with 1.49 eV excess energy), the carrier distribution was fitted with a Gaussian function, yielding a variance σ_0^2 of 350 ± 10 nm which is much larger than that of 260 nm ± 5 of the instrument response function (IRF). HC travel distance within the pulse duration was calculated to be 230 ± 16 nm using $\sqrt{\sigma_0^2 - IRF^2}$. In contrast, negligible HC travel within the time of pulse width was observed for photoexcitation with reduced excess energy (1.97eV pump, Figure 9a lower panel). The long HC travel distance within the pulse duration was attributed to quasi-ballistic transport for HCs arising from the large initial kinetic energies. Within 300 fs, the ~230 nm quasi-ballistic transport length for $MAPbI_3$ is much longer than ~20 nm for Si,[118] ~85 nm for GaAs,[119] and ~14 nm for GaN.[120] The authors attributed such phenomenon to the slower momentum relaxation in $MAPbI_3$ than in conventional semiconductors.

HC transport during HC-cooling was also established using TAM. Figure 9d shows the time-dependent σ_t^2 obtained from TAM image at longer decay time (Figure 9c). Under 1.97-eV photoexcitation, σ_t^2 increases linearly with delay time >1 ps, indicating diffusive transport of thermal equilibrium carriers as described by $\sigma_t^2 - \sigma_0^2 = 2Dt$. However, under 3.14-eV photoexcitation, such diffusive transport was only observed after ~30 ps until HCs travel ~600

nm before reaching thermal equilibrium with the lattice (Figure 9b). The nonequilibrium transport over tens of ps by such HCs is also much longer than those for only a few ps in the conventional semiconductors such as Si and GaAs.[121, 122] The authors attributed the long-lived and non-diffusive transport to the large polaron formation proposed by Zhu *et al.*[76] The calculated effective diffusion constant by $\frac{\Delta\sigma_t^2}{2\Delta t}$ for the 3.14-eV excitation is as large as 450 ± 10 cm^2 s^{-1} at ~1 ps, which decreases to an equilibrium value of 0.7 ± 0.1 cm^2s^{-1} (Figure 9d). Such a large initial diffusion constant of HCs induces the initial fast transport to long distance. This seminal experiment firmly established the potential of halide perovskites for HCSC applications.

6.2 Efficient HC Extraction

Efficient HC extraction is another litmus test for practical perovskite HCSC. HC extraction must be extremely fast because the rate of extraction is in competition with the rate of cooling rather than the carrier recombination rate. Furthermore, the thickness of the perovskite absorber must lie within the range HC transport distance. Li *et al.* first demonstrated efficient HC extraction from perovskites $MAPbBr_3$ NCs films.[9] Note that our $MAPbBr_3$ NC diameter is ~5 nm, which is in the realm of weak-intermediate confinement as $MAPbBr_3$ Bohr diameter is ~4 nm. To ensure that only HCs are extracted, narrow electron bandwidth semiconducting molecular Bphen (4,7-diphenyl-1,10-phenanthroline) was selected as the energy selective hot-electron extraction layer. Ultraviolet photoelectron spectroscopy (UPS) measurements (**Figure 10**a left) verify that Bphen's lowest unoccupied molecular orbital level (LUMO) is higher than the conduction band minimum (CBM) of $MAPbBr_3$ NCs. Before evaporating Bphen on the NCs-film (thickness of ~35 nm, Figure 10a right), ligand exchange between the long chain insulating oleic acid ligands on the as-prepared $MAPbBr_3$ NC surfaces with the short EDT (1,2-ethanedithiol) ligands was performed to improve the effective electronic

coupling between Bphen and NCs.

Using TA spectroscopy, the authors verified the occurrence of hot electron extraction in the EDT-NCs/Bphen films from: (i) the reduced high energy tails of the bandedge photobleaching (PB) band (+ΔT/T) of EDT-NCs (Figure 10b); (ii) the reduced PB amplitudes (Figure 10b inset) and (iii) the reduced initial HC temperature from ~1300 to 450 K within ~200 fs after photoexcitation (Figure 10c), as compared to the bare EDT-NCs films (without Bphen). We estimated the HC extraction efficiency (η_{hot}) based on the percentage reduction of the band edge PB intensities at ~ 0.8 ps (when the HCs are relaxed to the band edges) (Figure 10b inset). For $<N_0>$ ~0.1, the η_{hot} for EDT-NCs/Bphen is ~72 %. With annealing, even higher η_{hot} (up to~83%) was demonstrated. Comparatively, due to the faster HC cooling, the η_{hot} of its bulk-film counterpart is approximately 5 times lower under similar photoexcitation conditions. Consistently, η_{hot} reduces with (i) reducing excess HC energies, or (ii) reduces with increasing NC film thickness (from ~35 to 140 nm (Figure 10d)). We attributed the reduction in the hot-electron extraction to the limited HC diffusion/hopping distances within the NCs films. More recently, HC-extraction evidenced using the TA approach was also reported for a $CsPbI_3$ film with P3HT as the extraction layer by Shen *et al.*[38] The near instantaneous disappearance of the hot-energy tail (within ~0.3 ps) and the reduction of HC temperatures in $CsPbI_3$/P3HT bilayers validate the efficient and extremely fast hot-hole injection into P3HT (Figure 10e).

Using time-resolved terahertz spectroscopy (TRTS), Sarkar *et al.* also recently reported ultrafast HC transfer (sub-300 fs) in $CsPbBr_3$ NCs interfaced with benzoquinone molecules (electron acceptor) or phenothiazine (PTZ) molecules (hole acceptor).[123] TRTS is a very useful noncontact photoconductivity probe to investigate the HC transfer kinetics in NCs system.[124-126] Essentially, evidence of HC transfer from NCs to molecular acceptors is

derived from the difference between the transient THz photoconductivity spectra of NC/charge acceptor film and the neat NC film. At a diameter ~11 nm, their $CsPbBr_3$ NCs have almost no confinement effects since $CsPbBr_3$ Bohr diameter is ~7nm. The disappearance of the two phonon-resonance modes at~1.8 and ~3 THz in conductivity spectra (*i.e.*, due to HC-phonon interactions present in neat NCs [123, 127, 128]) for NCs/acceptor complex (for example for NC/PTZ system) (Figure 10f) suggests that HC transfer is faster than HC relaxation to the band edges. Do note that in their experiments, the energy levels of the extraction layers lie in between $CsPbBr_3$ bandgap. Consequently, the authors also observed a secondary transfer of cooled carriers at the bandedge to the charge extraction molecules.

In summary, these pioneering works provide important validation on the feasibility of HC extraction from halide perovskites. Nonetheless, they are primarily based on spectroscopy techniques. Moving forward, more direct electrical measurements on HC extraction are needed.

7. Challenges and Opportunities for Perovskite HCSCs

Recently, a prototype HCSC device based on III–V semiconductor QW as the absorber material was experimentally demonstrated (**Figure 11**a).[129] Nguyen *et al.*[129] fabricated a HC heterojunction device with intrinsic InGaAsP-based absorber consisting of a 7.4 nm QW (E_g = 0.78 eV) between 120 and 130 nm barriers (E_g = 1.05 eV, acting as hot-carrier selective energy contact SEC). The population and temperature of hot-carriers were probed using luminescence measurements (Figure 11b). Their IV measurements further revealed an increased electrochemical potential in the barrier along with increasing laser pump fluence (Figure 11c). This demonstration provides strong motivation and guidance for fabricating prototype perovskite HCSCs. On this basis, we examine the challenges and opportunities for perovskite HCSCs.

7.1 Selective Energy Contacts

Practical HCSC requires not only considerable retardation of the HC cooling process in the absorber layer but also efficient extraction of HCs from the device through a SEC. Finding a suitable candidate is a major challenge. An ideal SEC consists of a tunneling barrier with a resonant level that only accepts a very narrow range of energies ($\delta E << k_B T$), beyond which all electrons are reflected back into the HC absorbers.[14, 130, 131] Such SEC can protect the HCs from mixing with cold carriers in the contacts so as to minimize the entropy production during extraction, *i.e.*, allowing isentropic extraction of HCs (Figure 11d). Candidate SEC materials include wide bandgap semiconductors with narrow conduction and valence bands such as organic molecules, quantum well or dots with discrete energy levels etc.[13],[132] This narrow band SEC concept also imposes an additional requirement on the HC absorber material: *i.e.*, the absorber must possess highly efficient carrier-carrier scattering properties to enable renormalization of the carriers with energies above and below the SEC to allow extraction.[129] Such requirement can be eased with the semi-SEC concept (*i.e.*, $\delta E >> k_B T$, functioning as a high-pass filter for hot-carriers) using wide bandgap semiconductors with bandgaps larger than absorbers.[133] The calculated power conversion efficiency for HCSCs with semi-SEC can still achieve ~60% as compared to ~70% for HCSCs with ideal narrow bandpass SEC.[134] Nonetheless, given the absorber material will absorb photons over the broad solar spectrum, a key concern is whether the HCs are harvested at the SECs at expense of the "cold carriers" (near the bandedge) that will also be inadvertently present in the absorber layer. Solving this issue may require a radical rethinking of the device architecture (such as patterning/templating the SEC) which will further complicate the already complex device fabrication requirements of HCSC.

7.2 ETA-HCSC

Apart from the above SEC issue, a well-designed HCSC must also collect as much of the HCs at high temperatures as quickly as possible, since the higher the temperature of the extracted HCs, the higher is the HCSC efficiency (Figure 1d). Hence, HCSC should be electrically thin while optically thick (Figure 11e) to ensure that the HCs at their highest possible temperatures can be collected within a reasonable time (or distance). Although a slower HC cooling rate is essential for higher extraction probability, longer HC cooling lifetimes should not be superficially taken as the potential for higher HCSC efficiency. The extremely thin absorber (ETA) layer solar cell concept is highly relevant for halide perovskites given their large absorption coefficient. Low dimensional perovskite nanostructures[2,135,136] will be particularly well-suited for implementing perovskite HCSCs. ETA-HCSCs are conceptually similar to the dye-sensitized nano-heterojunctions (*e.g.*, using mesoporous TiO_2,[137, 138] TiO_2 nanotubes,[139] or ZnO nanowire arrays[140] as electrodes), where the molecular dye is now substituted with an extremely thin (tens of nm) layer of a perovskite polycrystalline or NCs film, with the SECs sandwiched between perovskite absorber and electrodes. In addition, the ETA-HCSC concept can also benefit from enhanced light trapping and anti-reflection effect due to the enlargement of surfaces and multiple light scattering arising from the nanostructured framework.[136]

7.3 Concentrator-HCSC

More intense illumination via concentrating the sun irradiation to a photovoltaic cell (*i.e.*, concentrator solar cells) have been demonstrated in Si, GaAs multi-junction cells to increase the conversion efficiency (Figure 11f).[141-143] Importantly, the hot-phonon bottleneck, Auger-heating, and/or band-filling effects in halide perovskites will enable the HC temperatures and lifetimes to be greatly increased under high excitation fluence. Therefore, deployment of halide perovskites in concentrator-HCSCs is a viable approach to improving the HCSCs efficiencies, particularly in the regime of low concentrator photovoltaics (up to 100 suns).

Another advantage of concentrator-HCSC is that the increased voltage-to-current can decrease the resistive losses under the high current densities of concentrator cells. Nevertheless, under increased illumination levels, halide perovskite material integrity and device stabilities will be a major challenge, especially for medium (100-300 suns) to high concentration (500-1000 suns) photovoltaics.[144] Thermal management with active/passive cooling may be necessary even for low concentrator halide perovskite photovoltaics.

8. Conclusions and Outlook

The slow hot-carrier cooling properties of halide perovskites show great promise to spin-off a new branch in perovskite hot-carrier solar cells and/or concentrator solar cells. In this first review on slow hot-carrier cooling in halide perovskites, we showcase this novel phenomenon and examine the seminal works. Ultrafast optical spectroscopy has played a key role in validating and deciphering the photophysics. Key findings include: long hot-carrier cooling lifetimes (up to 1 ns), long-range hot-carrier transport (up to ~600 nm) and highly efficient hot-carrier extraction (up to ~83%). This fledging area has made good headway in understanding the origins of slow hot-carrier cooling, with several fluence-dependent mechanisms proposed: large polarons, phonon bottleneck, acoustic phonon up-conversion, state-filling, and Auger-heating *etc*. Nonetheless, knowledge gaps remain, for instance in the contrasting trends over the elucidated hot carrier temperatures spanning the range of excitation densities. This could partly be traced to the intricacies between the different models used in estimating the temperatures. Further research is warranted. Apart from tracing the developmental milestones and distilling the complex photophysics, we also attempted to put together a rudimentary toolkit for engineering slow hot carrier cooling in halide perovskites and for the design of even more efficient HC perovskite absorbers. Presently, this phenomenon has been extensively investigated with short pulse lasers, more studies with CW

and even broadband stimuli are urgently needed to understand the intermixing of carriers in the absorber material. Lastly, device challenges and opportunities over the choice and application of the selective energy contacts and the ETA and concentrator concepts were highlighted. As halide perovskites continue to capture our imagination with their extraordinary properties, only time will tell if they can translate to disruptive technologies that transform our lives.

Acknowledgments

Financial support from Nanyang Technological University start-up grant M4080514; JSPS-NTU Joint Research Project M4082176; the Ministry of Education AcRF Tier 1 grant RG173/16 and Tier 2 grants MOE2015-T2-2-015 and MOE2016-T2-1-034; and from the Singapore National Research Foundation through the Competitive Research Programme NRF-CRP14-2014-03 and the NRF Investigatorship Programme NRF-NRFI-2018-04 are gratefully acknowledged.

Received: ((will be filled in by the editorial staff))
Revised: ((will be filled in by the editorial staff))
Published online: ((will be filled in by the editorial staff))

References

[1] H. P. Zhou, Q. Chen, G. Li, S. Luo, T. B. Song, H. S. Duan, Z. R. Hong, J. B. You, Y. S. Liu, Y. Yang, *Science* **2014**, *345*, 542.

[2] M. M. Lee, J. Teuscher, T. Miyasaka, T. N. Murakami, H. J. Snaith, *Science* **2012**, *338*, 643.

[3] N. J. Jeon, J. H. Noh, W. S. Yang, Y. C. Kim, S. Ryu, J. Seo, S. I. Seok, *Nature* **2015**, *517*, 476.

[4] J.-P. Correa-Baena, A. Abate, M. Saliba, W. Tress, T. Jesper Jacobsson, M. Grätzel, A. Hagfeldt, *Energy Environ. Sci.* **2017**, *10*, 710.

[5] National Renewable Energy Laboratory (NREL). Research Cell Efficiency Record. https://www.nrel.gov/pv/assets/images/efficiency-chart.png, accessed April, 2018.

[6] R. T. Ross, A. J. Nozik, *J. Appl. Phys.* **1982**, *53*, 3813.

[7] T. C. Sum, N. Mathews, G. Xing, S. S. Lim, W. K. Chong, D. Giovanni, H. A. Dewi, *Acc. Chem. Res.* **2016**, *49*, 294.

[8] G. Xing, N. Mathews, S. Sun, S. S. Lim, Y. M. Lam, M. Grätzel, S. Mhaisalkar, T. C. Sum, *Science* **2013**, *342*, 344.

[9] M. J. Li, S. Bhaumik, T. W. Goh, M. S. Kumar, N. Yantara, M. Grätzel, S. Mhaisalkar, N. Mathews, T. C. Sum, *Nat. Commun.* **2017**, *8*, 14350.

[10] K. Miyata, D. Meggiolaro, M. T. Trinh, P. P. Joshi, E. Mosconi, S. C. Jones, F. De Angelis, X.-Y. Zhu, *Sci. Adv.* **2017**, *3*, e1701217.

[11] M. A. Green, *Prog. Photovoltaics* **2001**, *9*, 123.

[12] M. A. Green, *Third generation photovoltaics: advanced solar energy conversion*, Springer Science & Business Media, **2006**.

[13] G. Conibeer, *Mater. Today* **2007**, 10, 42.

[14] D. Konig, K. Casalenuovo, Y. Takeda, G. Conibeer, J. F. Guillemoles, R. Patterson, L. M. Huang, M. A. Green, *Physica E* **2010**, *42*, 2862.

[15] Y. Takeda, T. Ito, T. Motohiro, D. Konig, S. Shrestha, G. Conibeer, *J. Appl. Phys.* **2009**, *105*, 074905.

[16] M. C. Hanna, A. J. Nozik, *J. Appl. Phys.* **2006**, 100, 074510.

[17] J. H. Werner, S. Kolodinski, H. J. Queisser, *Phys. Rev. Lett.* **1994**, 72, 3851.

[18] R. D. Schaller, V. I. Klimov, *Phys. Rev. Lett.* **2004**, 92, 186601.

[19] M. J. Li, R. Begum, J. Fu, K. T. Ming, S. A Veldhuis, M. Grätzel, N. Mathews, S. Mhaisalkar, T. C. Sum, *Nat. Commun.*, DOI: 10.1038/s41467-018-06596-1.

[20] J. Y. Kim, K. Lee, N. E. Coates, D. Moses, T-Q. Nguyen, M. Dante, A. J. Heeger, *Science* **2007**, 317, 222.

[21] B. Chen, Y. Bai, Z. Yu, T. Li, X. Zheng, Q. Dong, L. Shen, M. Boccard, A. Gruverman, Z. Holman, J. Huang *Adv. Energy Mater.* **2016**, 6, 1601128.

[22] Y. Yang, D. P. Ostrowski, R. M. France, K. Zhu, J. Van De Lagemaat, J. M. Luther, M. C. Beard, *Nat. Photonics* **2016**, *10*, 53.

[23] Y. C. Wen, C. Y. Chen, C. H. Shen, S. Gwo, C. K. Sun, *Appl. Phys. Lett.* **2006**, 89, 232114.

[24] G. C. A. Nozik, M. C. Beard *Advanced Concepts in Photovoltaics*, Royal Society of Chemistry, UK **2014**.

[25] G. J. Conibeer, D. Konig, M. A. Green, J. F. Guillemoles, *Thin Solid Films* **2008**, *516*, 6948.

[26] M. A. Green, K. Emery, Y. Hishikawa, W. Warta, E. D. Dunlop, *Prog. Photovoltaics Res. Appl.* **2015**, *23*, 1.

[27] H. Cho, S.-H. Jeong, M.-H. Park, Y.-H. Kim, C. Wolf, C.-L. Lee, J. H. Heo, A. Sadhanala, N. Myoung, S. Yoo, *Science* **2015**, *350*, 1222.

[28] J. M. Richter, F. Branchi, F. V. de Almeida Camargo, B. Zhao, R. H. Friend, G. Cerullo, F. Deschler, *Nat. Commun.* **2017**, *8*, 376.

[29] J. Fu, Q. Xu, G. Han, B. Wu, C. H. A. Huan, M. L. Leek, T. C. Sum, *Nat. Commun.* **2017**, *8*, 1300.

[30] J. Yang, X. Wen, H. Xia, R. Sheng, Q. Ma, J. Kim, P. Tapping, T. Harada, T. W. Kee, F. Huang, *Nat. Commun.* **2017**, *8*, 14120.

[31] H. Zhu, K. Miyata, Y. Fu, J. Wang, P. P. Joshi, D. Niesner, K. W. Williams, S. Jin, X.-Y. Zhu, *Science* **2016**, *353*, 1409.

[32] A. Moliton, *Solid-State physics for electronics*, Wiley, Hoboken, NJ, USA **2009**.

[33] G. Grancini, M. Maiuri, D. Fazzi, A. Petrozza, H. J. Egelhaaf, D. Brida, G. Cerullo, G. Lanzani, *Nat. Mater.* **2013**, *12*, 29.

[34] A. E. Jailaubekov, A. P. Willard, J. R. Tritsch, W. L. Chan, N. Sai, R. Gearba, L. G. Kaake, K. J. Williams, K. Leung, P. J. Rossky, X. Y. Zhu, *Nat. Mater.* **2013**, *12*, 66.

[35] T. C. Sum, N. Mathews, *Energy Environ. Sci.* **2014**, *7*, 2518.

[36] K. Chen, A. J. Barker, F. L. Morgan, J. E. Halpert, J. M. Hodgkiss, *J. Phys. Chem. Lett.* **2014**, *6*, 153.

[37] H. Kawai, G. Giorgi, A. Marini, K. Yamashita, *Nano Lett.* **2015**, *15*, 3103.

[38] Q. Shen, T. S. Ripolles, J. Even, Y. Zhang, C. Ding, F. Liu, T. Izuishi, N. Nakazawa, T. Toyoda, Y. Ogomi, *J. Energy Chem.* **2018**, 27, 1170.

[39] J. C. Brauer, Y. H. Lee, M. K. Nazeeruddin, N. Banerji, *J. Mater. Chem. C* **2016**, *4*, 5922.

[40] S. A. Bretschneider, F. Laquai, M. Bonn, *J. Phys. Chem. C* **2017**, *121*, 11201.

[41] A. Y. Chang, Y. J. Cho, K. C. Chen, C. W. Chen, A. Kinaci, B. T. Diroll, M. J. Wagner, M. K. Chan, H. W. Lin, R. D. Schaller, *Adv. Energy Mater.* **2016**, 6, 1600422.

[42] Z. Guo, Y. Wan, M. Yang, J. Snaider, K. Zhu, L. Huang, *Science* **2017**, 356, 59.

[43] H.-H. Fang, S. Adjokatse, S. Shao, J. Even, M. A. Loi, *Nat. Commun.* **2018**, *9*, 243.

[44] Q. Shen, T. S. Ripolles, J. Even, Y. Ogomi, K. Nishinaka, T. Izuishi, N. Nakazawa, Y. Zhang, C. Ding, F. Liu, *Appl. Phys. Lett.* **2017**, *111*, 153903.

[45] E. M. Talbert, H. F. Zarick, A. Boulesbaa, N. Soetan, A. A. Puretzky, D. B. Geohegan, R. Bardhan, *Nanoscale* **2017**, *9*, 12005.

[46] J. Fu, Q. Xu, G. Han, B. Wu, C. H. A. Huan, M. L. Leek, T. C. Sum, *Nat. Commun.* **2017**, *8*, 1300.

[47] M. B. Price, J. Butkus, T. C. Jellicoe, A. Sadhanala, A. Briane, J. E. Halpert, K. Broch, J. M. Hodgkiss, R. H. Friend, F. Deschler, *Nat. Commun.* **2015**, *6*, 8420.

[48] P. Papagiorgis, L. Protesescu, M. V. Kovalenko, A. Othonos, G. Itskos, *J. Phys. Chem. C* **2017**, *121*, 12434.

[49] M. E. Madjet, G. R. Berdiyorov, F. El-Mellouhi, F. H. Alharbi, A. V. Akimov, S. Kais, *J. Phys. Chem. Lett.* **2017**, *8*, 4439.

[50] S. Nah, B. Spokoyny, C. M. Soe, C. Stoumpos, M. G. Kanatzidis, E. Harel, *Nano Lett.* **2018**, *18*, 1044.

[51] J. Butkus, P. Vashishtha, K. Chen, J. K. Gallaher, S. K. Prasad, D. Z. Metin, G. Laufersky, N. Gaston, J. E. Halpert, J. M. Hodgkiss, *Chem. Mater.* **2017**, *29*, 3644.

[52] K. Chen, A. J. Barker, F. L. Morgan, J. E. Halpert, J. M. Hodgkiss, *J. Phys. Chem. Lett* **2014**, *6*, 153.

[53] M. Achermann, A. P. Bartko, J. A. Hollingsworth, V. I. Klimov, *Nat. Phys.* **2006**, *2*, 557.

[54] V. Klimov, P. H. Bolivar, H. Kurz, *Phys. Rev. B* **1995**, *52*, 4728.

[55] F. Chen, A. N. Cartwright, H. Lu, W. J. Schaff, *Appl. Phys. Lett.* **2003**, *83*, 4984.

[56] S. A. Bretschneider, F. Laquai, M. Bonn, *J. Phys. Chem. C* **2017**, *121*, 11201.

[57] P. Papagiorgis, L. Protesescu, M. V. Kovalenko, A. Othonos, G. Itskos, *J. Phys. Chem. C* **2017**, *121*, 12434.

[58] S. Prabhu, A. S. Vengurlekar, *Phys. Rev. B* **1996**, *53*, 7815.

[59] S. Prabhu, A. S. Vengurlekar, S. Roy, J. Shah, *Phys. Rev. B* **1995**, *51*, 14233.

[60] C. K. Choi, Y. H. Kwon, J. S. Krasinski, G. H. Park, G. Setlur, J. J. Song, Y. C. Chang, *Phys. Rev. B* **2001**, *63*, 115315.

[61] S. E. Kumekov, V. I. Perel, Sov. Phys. *J. Exp. Theor. Phys* **1988**, *67*, 193.

[62] J. F. Ryan, R. A. Taylor, A. J. Turberfield, Angela Maciel, J. M. Worlock, A. C. Gossard, W. Wiegmann, *Phys. Rev. Lett.* **1984**, *53*, 1841.

[63] R. F. Leheny, J. Shah, R. L. Fork, C. V. Shank, A. Migus, *Solid State Commun.* **1979**, *31*, 809.

[64] D. Von der Linde, R. Lambrich, *Phys. Rev. Lett.* **1979**, *42*, 1090.

[65] H. M. Zhu, K. Miyata, Y. P. Fu, J. Wang, P. P. Joshi, D. Niesner, K. W. Williams, S. Jin, X. Y. Zhu, *Science* **2016**, *353*, 1409.

[66] J. R. Goldman, J. A. Prybyla, *Phys. Rev. Lett.* **1994**, *72*, 1364.

[67] P. Umari, E. Mosconi, F. De Angelis, *Sci. Rep.* **2014**, *4*, 4467.

[68] A. Caretta, M. C. Donker, D. W. Perdok, D. Abbaszadeh, A. O. Polyakov, R. W. A. Havenith, T. T. M. Palstra, P. H. M. van Loosdrecht, *Phys. Rev. B* **2015**, *91*, 054111.

[69] S. T. Ha, C. Shen, J. Zhang, Q. H. Xiong, *Nat. Photonics* **2015**, *10*, 115.

[70] M. Achermann, A. P. Bartko, J. A. Hollingsworth, V. I. Klimov, *Nat. Phys.* **2006**, *2*, 557.

[71] M. C. Downer, C. V. Shank, *Phys. Rev. Lett.* **1986**, *56*, 761.

[72] A. Haug, *J. Phys. C Solid State Phys.* **1983**, *16*, 4159.

[73] P. Borri, S. Ceccherini, M. Gurioli, F. Bogani, *Solid State Commun.* **1997**, *103*, 77.

[74] C. Wehrenfennig, M. Z. Liu, H. J. Snaith, M. B. Johnston, L. M. Herz, *J. Phys. Chem. Lett.* **2014**, *5*, 1300.

[75] K. Miyata, T. L. Atallah, X. Y. Zhu, *Sci. Adv*. **2017**, *3*, e1701469.

[76] D. Niesner, H. M. Zhu, K. Miyata, P. P. Joshi, T. J. S. Evans, B. J. Kudisch, M. T. Trinh, M. Marks, X. Y. Zhu, *J. Am. Chem. Soc.* **2017**, *139*, 6777.

[77] Y. Chen, H. T. Yi, X. Wu, R. Haroldson, Y. N. Gartstein, Y. I. Rodionov, K. S. Tikhonov, A. Zakhidov, X. Y. Zhu, V. Podzorov, *Nat. Commun.* ***2016***, *7*, 12253.

[78] X. Y. Zhu, V. Podzorov, *J. Phys. Chem. Lett.* **2015**, *6*, 4758.

[79] J. M. Frost, A. Walsh, *Acc. Chem. Res.* **2016**, *49*, 528.

[80] D. Mcmorrow, W. T. Lotshaw, G. A. Kenney-Wallace, *IEEE J. Quantum Electron.* **1988**, *24*, 443.

[81] R. Righini*, Science* **1993**, *262*, 1386.

[82] T. J. Savenije, C. S. Ponseca, L. Kunneman, M. Abdellah, K. B. Zheng, Y. X. Tian, Q. S. Zhu, S. E. Canton, I. G. Scheblykin, T. Pullerits, A. Yartsev, V. Sundstrom, *J. Phys. Chem. Lett.* **2014**, *5*, 2189.

[83] H. T. Yi, X. X. Wu, X. Y. Zhu, V. Podzorov, *Adv. Mater.* **2016**, *28*, 6509.

[84] A. Pisoni, J. Jaćimović, O. S. Barišić, M. Spina, R. Gaál, L. Forró, E. Horváth, *J. Phys. Chem. Lett.* **2014**, *5*, 2488.

[85] A. Kovalsky, L. L. Wang, G. T. Marek, C. Burda, J. S. Dyck, *J. Phys. Chem. C* **2017**, *121*, 3228.

[86] Z. Guo, S. J. Yoon, J. S. Manser, P. V. Kamat, T. F. Luo, *J. Phys. Chem. C* **2016**, *120*, 6394.

[87] J. M. Frost, L. D. Whalley, A. Walsh, *ACS Energy Lett.* **2017**, *2*, 2647.

[88] J. S. Manser, P. V. Kamat, *Nat. Photonics* **2014**, *8*, 737.

[89] A. J. Nozik, *Annu. Rev. Phys. Chem.* **2001**, *52*, 193.

[90] U. Bockelmann, G. Bastard, *Phys. Rev. B* **1990**, *42*, 8947.

[91] H. Benisty, C. M. Sotomayortorres, C. Weisbuch, *Phys. Rev. B* **1991**, *44*, 10945.

[92] A. L. Efros, V. A. Kharchenko, M. Rosen, *Solid State Commun.* **1995**, *93*, 281.

[93] E. Hendry, M. Koeberg, F. Wang, H. Zhang, C. de Mello Donegá, D. Vanmaekelbergh, M. Bonn, *Phys. Rev. Lett.* **2006**, *96*, 057408.

[94] S. V. Kilina, D. S. Kilin, O. V. Prezhdo, *ACS Nano* **2009**, *3*, 93.

[95] J. L. Blackburn, R. J. Ellingson, O. I. Mićić, A. J. Nozik, *J. Phys. Chem. B* **2003**, *107*, 102.

[96] W. J. Yin, J. H. Yang, J. Kang, Y. F. Yan, S. H. Wei, *J. Mater. Chem. A* **2015**, *3*, 8926.

[97] S. T. A. G. Melissen, F. Labat, P. Sautet, T. Le Bahers, *Phys. Chem. Chem. Phys.* **2015**, *17*, 2199.

[98] V. I. Klimov, *J. Phys. Chem. B* **2000**, *104*, 6112.

[99] V. I. Klimov, D. W. McBranch, *Phys. Rev. Lett.* **1998**, *80*, 4028.

[100] V. I. Klimov, A. A. Mikhailovsky, D. W. McBranch, C. A. Leatherdale, M. G. Bawendi, *Science* **2000**, *287*, 1011.

[101] S. Chatterjee, A. J. Pal, *J. Mater. Chem. A* **2018**, *6*, 3793.

[102] A. C. Ferreira, A. Létoublon, S. Paofai, S. Raymond, C. Ecolivet, B. Rufflé, S. Cordier, C. Katan, M. I. Saidaminov, A. A. Zhumekenov, O.M. Bakr, J. Even, Ph. Bourges, https://arxiv.org/abs/1801.08701 Jan, 2018.

[103] C. Shen, W. N. Du, Z. Y. Wu, J. Xing, S. T. Ha, Q. Y. Shang, W. G. Xu, Q. H. Xiong, X. F. Liu, Q. Zhang, *Nanoscale* **2017**, *9*, 8281.

[104] D. H. Fabini, T. A. Siaw, C. C. Stoumpos, G. Laurita, D. Olds, K. Page, J. G. Hu, M. G. Kanatzidis, S. G. Han, R. Seshadri, *J. Am. Chem. Soc.* **2017**, *139*, 16875.

[105] J. X. Liu, J. Leng, K. F. Wu, J. Zhang, S. Y. Jin, *J. Am. Chem. Soc.* **2017**, *139*, 1432.

[106] L. L. Wang, C. McCleese, A. Kovalsky, Y. X. Zhao, C. Burda, *J. Am. Chem. Soc.* **2014**, *136*, 12205.

[107] S. Nah, B. Spokoyny, C. M. Soe, C. C. Stoumpos, M. G. Kanatzidis, E. Harel, *Nano lett.* **2018**, *18*, 1044.

[108] J.-H. Im, I.-H. Jang, N. Pellet, M. Grätzel, N.-G. Park, *Nat. Nanotechnol.* **2014**, *9*, 927.

[109] S. A. Veldhuis, Y. K. E. Tay, A. Bruno, S. S. H. Dintakurti, S. Bhaumik, S. K. Muduli, M. Li, N. Mathews, T. C. Sum, S. G. Mhaisalkar, *Nano Lett.* **2017**, *17*, 7424.

[110] M. Imran, V. Caligiuri, M. Wang, L. Goldoni, M. Prato, R. Krahne, L. De Trizio, L. Manna, *J. Am. Chem. Soc.* **2018**, *140*, 2656.

[111] S. Bhaumik, S. A. Veldhuis, Y. F. Ng, M. Li, S. K. Muduli, T. C. Sum, B. Damodaran, S. Mhaisalkar, N. Mathews, *Chem. Commun.* **2016**, *52*, 7118.

[112] D. Tedeschi, M. De Luca, H. A. Fonseka, Q. Gao, F. Mura, H. H. Tan, S. Rubini, F. Martelli, C. Jagadish, M. Capizzi, A. Polimeni, *Nano Lett.* **2016**, *16*, 3085.

[113] M. M. Gabriel, J. R. Kirschbrown, J. D. Christesen, C. W. Pinion, D. F. Zigler, E. M. Grumstrup, B. P. Mehl, E. E. M. Cating, J. F. Cahoon, J. M. Papanikolas, *Nano Lett*. **2013**, *13*, 1336.

[114] Y. Wan, Z. Guo, T. Zhu, S. X. Yan, J. Johnson, L. B. Huang, *Nat. Chem.* **2015**, *7*, 785.

[115] M. K. L. Man, A. Margiolakis, S. Deckoff-Jones, T. Harada, E. L. Wong, M. B. M. Krishna, J. Madeo, A. Winchester, S. Lei, R. Vajtai, P. M. Ajayan, K. M. Dani, *Nat. Nanotechnol.* **2017**, *12*, 36.

[116] M. T. Trinh, X. X. Wu, D. Niesner, X. Y. Zhu, *J. Mater. Chem. A* **2015**, *3*, 9285.

[117] M. B. Price, J. Butkus, T. C. Jellicoe, A. Sadhanala, A. Briane, J. E. Halpert, K. Broch, J. M. Hodgkiss, R. H. Friend, F. Deschler, *Nat. Commun.* **2015**, *6*, 8420.

[118] M. Bernardi, D. Vigil-Fowler, J. Lischner, J. B. Neaton, S. G. Louie, *Phys. Rev. Lett.* **2014**, *112*, 257402.

[119] J. R. Hayes, A. F. J. Levi, *IEEE J. Quantum Electron.* **1986**, *22*, 1744.

[120] D. J. Suntrup, G. Gupta, H. R. Li, S. Keller, U. K. Mishra, *Appl. Phys. Lett.* **2014**, *105*, 26.

[121] B. B. Hu, E. A. Desouza, W. H. Knox, J. E. Cunningham, M. C. Nuss, A. V. Kuznetsov, S. L. Chuang, *Phys. Rev. Lett.* **1995**, *74*, 1689.

[122] C. V. Shank, R. L. Fork, R. F. Leheny, J. Shah, *Phys. Rev. Lett.* **1979**, *42*, 112.

[123] S. Sarkar, V. K. Ravi, S. Banerjee, G. R. Yettapu, G. B. Markad, A. Nag, P. Mandal, *Nano Lett.* **2017**, *17*, 5402.

[124] M. C. Beard, G. M. Turner, C. A. Schmuttenmaer, *J. Phys. Chem. A* **2002**, *106*, 878.

[125] R. Ulbricht, E. Hendry, J. Shan, T. F. Heinz, M. Bonn, *Rev. Mod. Phys.* **2017**, *89*, 029901.

[126] C. A. Schmuttenmaer, *Chem. Rev.* **2004**, *104*, 1759.

[127] C. Wehrenfennig, G. E. Eperon, M. B. Johnston, H. J. Snaith, L. M. Herz, *Adv. Mater.* **2014**, *26*, 1584.

[128] M. Karakus, S. A. Jensen, F. D'Angelo, D. Turchinovich, M. Bonn, E. Canovas, *J. Phys. Chem. Lett.* **2015**, *6*, 4991.

[129] D-T. Nguyen, L. Lombez, F. Gibelli, S. Boyer-Richard, A. L. Corre, O. Durand, J-F. Guillemoles, *Nat. Energy*, **2018**, 3, 236

[130] G. Conibeer, C.-W. Jiang, D. König, S. Shrestha, T. Walsh, M. Green, *Thin Solid Films* **2008**, *516*, 6968.

[131] G. Conibeer, M. Green, R. Corkish, Y. Cho, E. C. Cho, C. W. Jiang, T. Fangsuwannarak, E. Pink, Y. D. Huang, T. Puzzer, T. Trupke, B. Richards, A. Shalav, K. L. Lin, *Thin Solid Films* **2006**, *511*, 654.

[132] P. Wurfel, *Sol. Energ. Mat. Sol. C* **1997**, *46*, 43.

[133] A. L. Bris, J.-F. Guillemoles, *Appl. Phys. Lett.* **2010**, *97*, 113506.

[134] D.-T. Nguyen, L. Lombez, F. Gibelli, S. Boyer-Richard, A. Le Corre, O. Durand, J.-F. Guillemoles, *Nat. Energy* **2018**, *3*, 236.

[135] K. Ernst, A. Belaidi, R. Konenkamp, *Semicond. Sci. Technol.* **2003**, *18*, 475.

[136] M. Grätzel, *Nature* **2001**, *414*, 338.

[137] U. Bach, D. Lupo, P. Comte, J. E. Moser, F. Weissortel, J. Salbeck, H. Spreitzer, M. Grätzel, *Nature* **1998**, *395*, 583.

[138] D. H. Chen, F. Z. Huang, Y. B. Cheng, R. A. Caruso, *Adv. Mater.* **2009**, *21*, 2206.

[139] G. K. Mor, K. Shankar, M. Paulose, O. K. Varghese, C. A. Grimes, *Nano Lett.* **2006**, *6*, 215.

[140] M. Law, L. E. Greene, J. C. Johnson, R. Saykally, P. D. Yang, *Nat. Mater.* **2005**, *4*, 455.

[141] W. Guter, J. Schöne, S. P. Philipps, M. Steiner, G. Siefer, A. Wekkeli, E. Welser, E. Oliva, A. W. Bett, F. Dimroth, *Appl. Phys. Lett.* **2009**, *94*, 223504.

[142] M. D. Lammert, R. J. Schwartz, *IEEE Trans. Electron Devices* **1977**, *24*, 337.

[143] P. Perez-Higueras, E. Munoz, G. Almonacid, P. G. Vidal, *Renew Sust. Energ. Rev.* **2011**, *15*, 1810.

[144] F. Lang, O. Shargaieva, V. V. Brus, H. C. Neitzert, J. Rappich, N. H. Nickel, *Adv. Mater.* **2018**, *30*, 1702905.

Figures

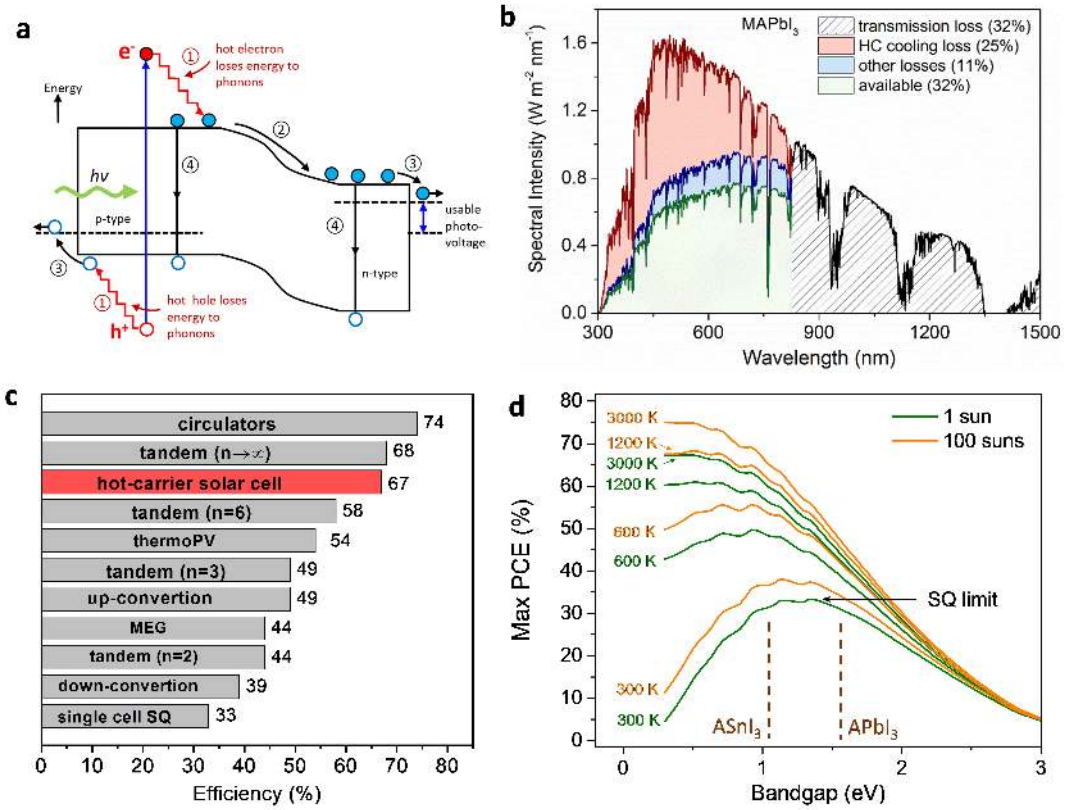

Figure 1. a) Main energy loss processes in a standard single-junction solar cell: ① HC cooling loss (red lines); ②, ③ junction and contact losses; ④ recombination loss. a) Adapted and reproduced with permission.[11] Copyright 2001, John Wiley & Sons, Ltd. b) Illustration of the intrinsic losses for a single junction perovskite solar cell with bandgap = 1.5 eV (e.g., $MAPbI_3$) over the solar spectrum. Other losses include emission, Carnot, and Boltzmann losses *etc*. c) The options for new generation solar cells with efficiencies higher than the SQ-limit. d) Detailed balance calculations for the ultimate efficiency of an ideal HCSC vs. carrier temperature and absorber bandgap under one- and 100-suns concentration of the solar irradiation (*i.e.*, low concentrator photovoltaics). The lowermost curve corresponds to that for conventional cells. The vertical dashed lines indicate the bandgap positions of perovskites. A in $ASnI_3$ and $APbI_3$ refers to the cations MA, FA or Cs.

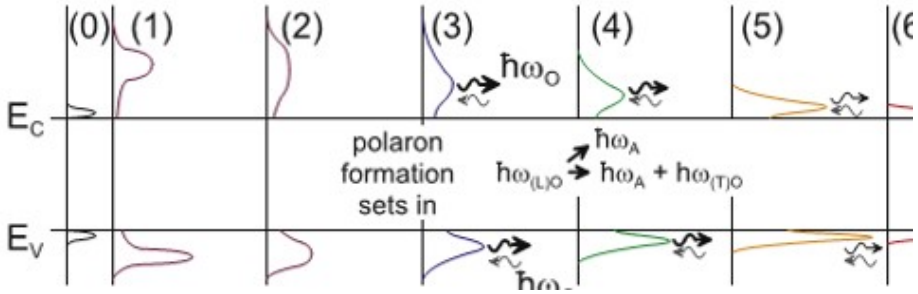

Figure 2. Schematic of the evolution of the carrier distribution with time after pulsed laser excitation. (0) thermal equilibrium state; (1) laser excitation; (2) carrier thermalization to Fermi-Dirac statistics; (3) carrier-optical phonon interactions; (4) decay of optical phonons into acoustic phonons; (5) further phonon emission to thermal equilibrium; (6) onset of carrier recombination. Reproduced with permission.[14] Copyright 2010, Elsevier.

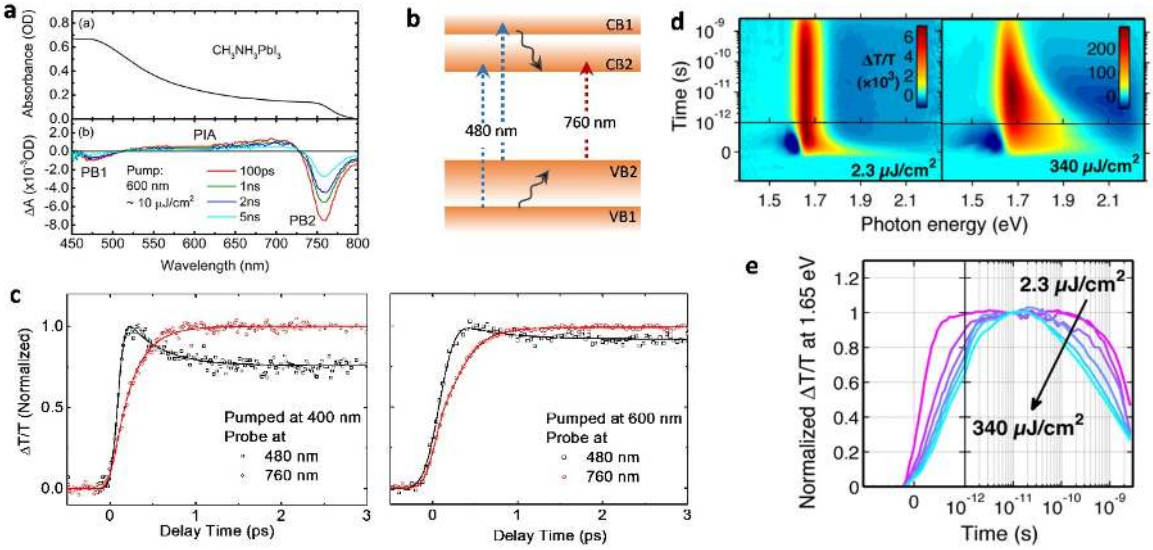

Figure 3. a) Linear absorption spectrum (upper panel) and TA spectra (lower panel) of $MAPbI_3$ showing the absorption edges at ~480 and ~760 nm at different probe delays. b) Schematic of the dual valence band and dual conduction band model showing the hot-hole cooling from VB1 and hot-electron cooling from CB1 (curly black arrows). c) Normalized TA dynamics probed at 480 and 760 nm in $MAPbI_3$ film after excitation at 400 nm (1 μJ cm^{-2}, left panel) and 600 nm (10 μJ cm^{-2}, right panel). a)-b) and right panel of c) are adapted and reproduced with permission. [7] Copyright 2016, American Chemical Society. Left panel of c) is adapted and reproduced with permission.[8] Copyright 2013, American Association for the Advancement of Science. d) Pseudo-color TA spectra of $MAPbI_{3-x}Cl_x$ film under 3.1-eV photoexcitation at low and high pump fluence. e) Normalized PB dynamics probed at 1.65 eV for the $MAPbI_{3-x}Cl_x$ film at different pump fluence under 3.1-eV photoexcitation. d)-e) Reproduced with permission.[52] Copyright 2014, American Chemical Society.

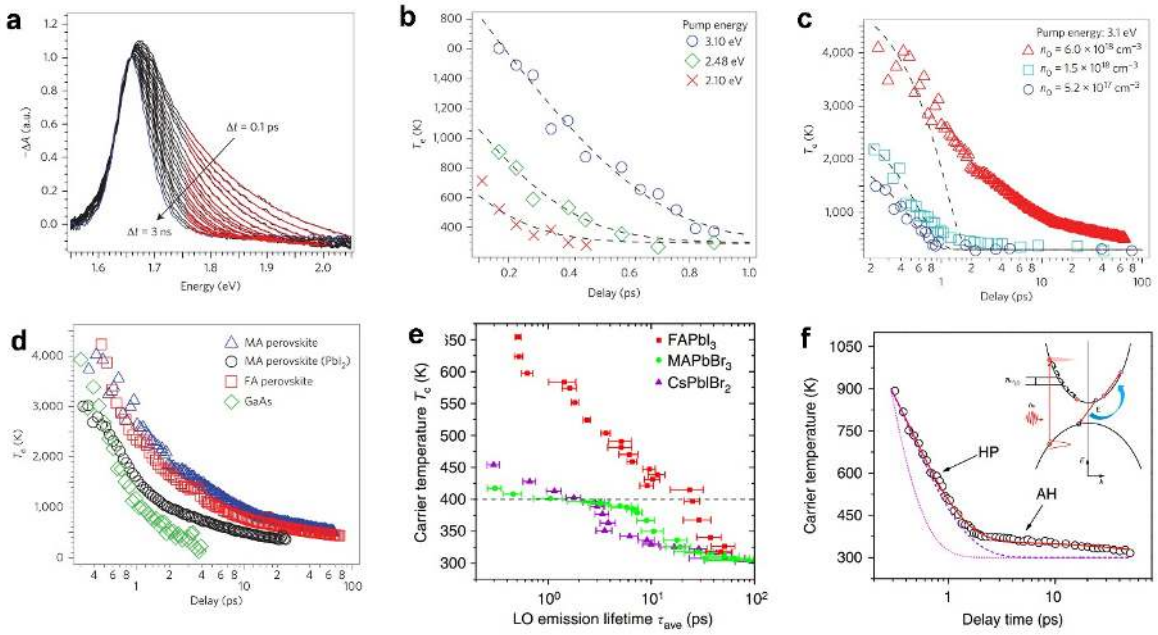

Figure 4. Slow HC cooling in perovskite films. a) Normalized TA spectrum at different delay times. Red curves are fittings using Equation (1) to obtain the HC temperature. b) HC cooling dynamics with a similar initial carrier density of 5.2×10^{17} cm^{-3} but with variable excitation energy. c) HC temperature as a function of delay time with variable initial carrier density. Dashed black curves in b) and c) are model fitting using Equation (2). d) HC cooling dynamics for perovskites and GaAs films with a similar initial carrier density of ~ 6.0×10^{18} cm^{-3}. a)-d) Reproduced with permission.[22] Copyright 2016, Nature Publishing Group. e) HC temperature dependence of LO-phonon emission lifetimes for various lead halide perovskites with a similar initial carrier density of ~ 2×10^{18} cm^{-3}. The error bars refer to the standard errors of the average lifetime of LO-phonon emission. Reproduced with permission.[30] Copyright 2017, Nature Publishing Group. f) HC cooling in the presence of hot-phonon (HP) and Auger-heating (AH) effect. Inset is a schematic of hot electron cooling in the presence of hot-phonon and Auger-heating effect. Reproduced with permission.[46] Copyright 2017, Nature Publishing Group.

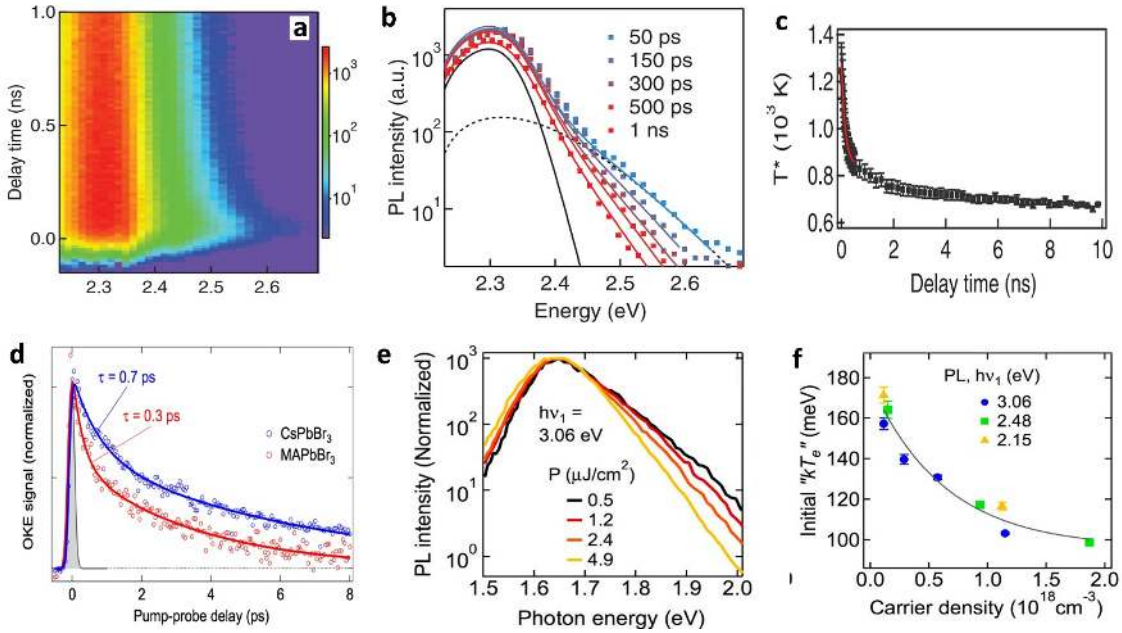

Figure 5. Long-lived HC emission. a) Pseudocolor (intensity) plot of TRPL spectra from a single crystal $MAPbBr_3$ microplate at a pump fluence of 1.7 μJ cm^{-2} and 3.08-eV excitation energy at room temperature. b) Transient PL spectra (squares) at different delay times with two-temperature model fittings (color curves). c) Extracted HC temperatures as a function of delay time, in which the red curve for the first 0.5 ns gives a HC relaxation time of 150 ± 30 ps. a)-c) Reproduced with permission.[65] Copyright 2016, American Association for the Advancement of Science. d) Normalized TR-OKE responses for $MAPbBr_3$ (red circles) and $CsPbBr_3$ (blue circles) single crystals under photoexcitation of 2.30 eV and 2.38 eV, respectively. Reproduced with permission.[75] Copyright 2016, American Association for the Advancement of Science. e) Normalized initial transient PL spectra under 3.06-eV photoexcitation and different pump fluence. f) Initial HC temperatures as a function of initial excitation density extracted from PL spectra at three excitation photon energies. e)-f) Reproduced with permission.[76] Copyright 2016, American Chemical Society.

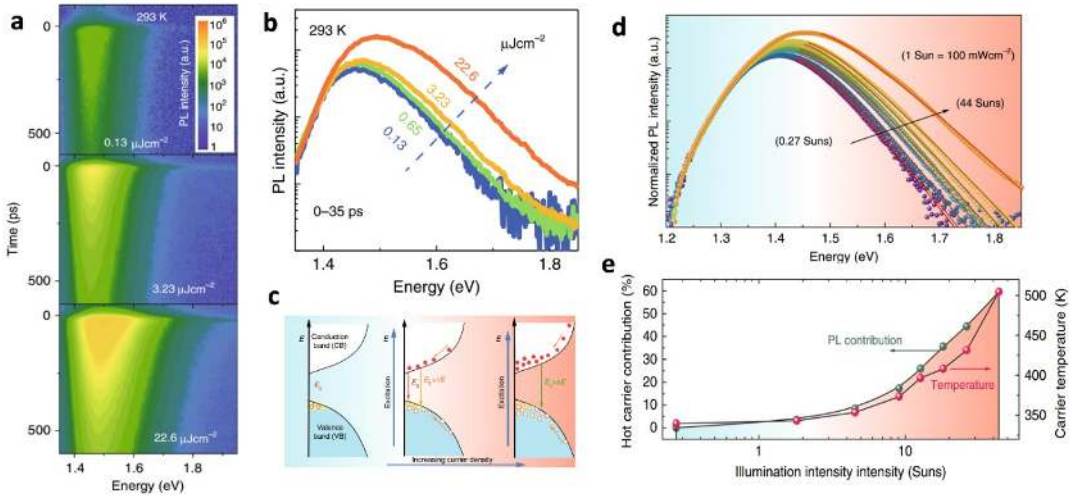

Figure 6. a) Pseudocolor (intensity) plot of TRPL spectra at different pump fluence of the $FASnI_3$ film under 3.1 eV photoexcitation at room temperature. b) Semi-log plot of initial transient PL spectra at different pump fluence. To show the HC PL clearly, the PL spectra are normalized at the low-energy tail. c) Schematic mechanism for the blue shift of the PL resulting from band-filling. d) PL spectra of the $FASnI_3$ film with the addition of SnF_2 under 405 nm CW-laser diode excitation at different pump fluence. e) HC contribution and carrier temperature versus illumination intensities in terms of the number of suns. a)-e) Reproduced with permission.[43] Copyright 2017, Nature Publishing Group.

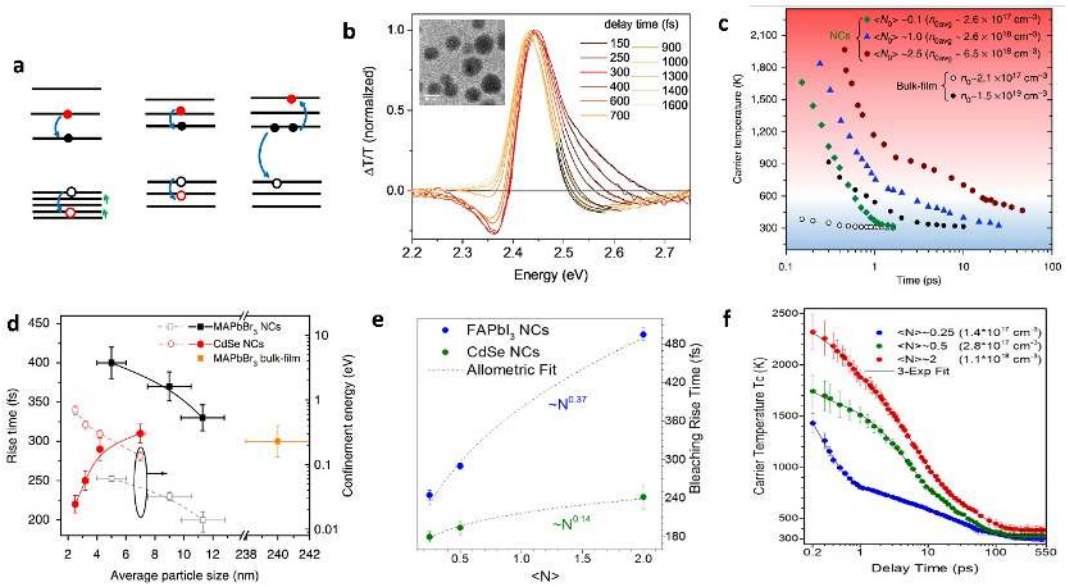

Figure 7. a) Schematic HC cooling via intraband Auger-type energy transfer in conventional II-VI semiconductor NCs with their dense hole states (also known as the hole manifold) (left); intrinsic phonon bottleneck effect with symmetric discrete energy levels (middle); Auger-heating (right) at high carrier density. b) Normalized TA spectra at a different delay time of colloidal $MAPbBr_3$ NCs with $<N_0>$~0.1 (following 3.1 eV photoexcitation), the solid black lines are Boltzmann fits to the high-energy tails. Inset: TEM image of NCs. c) HC temperature verses delay time for the $MAPbBr_3$ NCs and bulk-film under 3.1eV photoexcitation with carrier densities. d) NC size dependent band-edge bleaching rise time and related quantum confinement energies for perovskite NCs and CdSe NCs with initial electron-hole pair per NC ($<N_0>$) ~0.1. The rise time for perovskite bulk film excited with an equivalent fluence is also included for comparison. a)-d) Adapted and reproduced with permission.[9] Copyright 2017, Nature Publishing Group. e) Carrier density-dependent bleaching rise time for $FAPbI_3$ and CdSe NCs. f) HC temperature verses delay time under different carrier densities. e)-f) Reproduced with permission.[57] Copyright 2017, American Chemical Society.

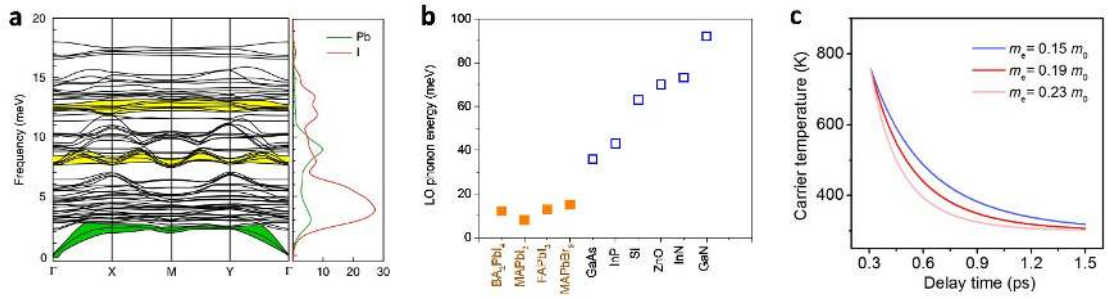

Figure 8. a) DFT calculated phonon energy spectra and projected phonon density of states of $MAPbI_3$. Yellow and green zones represent LO-phonon and acoustic phonon modes, respectively. b) Comparison of LO phonon energy for perovskites (solid squares) and conventional semiconductors (open squares). c) Calculated HC carrier cooling with different electron effective masses. a) and c) Adapted and reproduced with permission Reproduced with permission.[46] Copyright 2017 Nature Publishing Group.

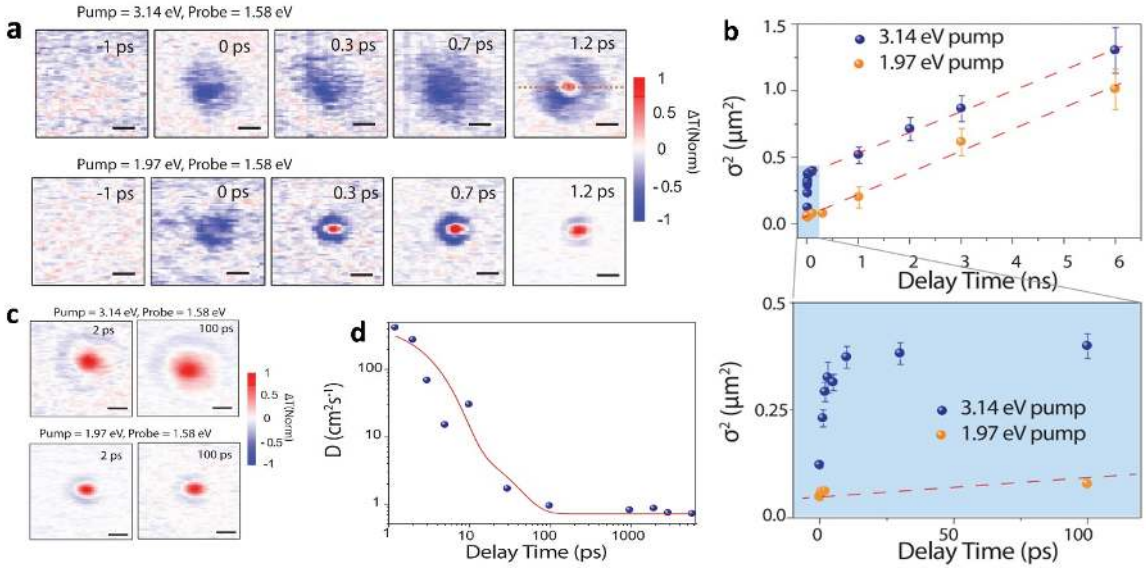

Figure 9. Imaging HC transport within 100 ps. a) TA microscopy images probed at 1.58 eV at different delay times under 3.14eV (upper panel) and 1.97eV (lower panel) photoexcitation. Scale bars, 1 µm. b) σ_t^2 versus delay time under 1.97eV and 3.14eV photoexcitation up to 6 ns (upper panel). Dashed linear fits indicate the diffusive transport. Zoomed-in view of b) for the first 100 ps delay time (lower panel). c) TA microscopy images at longer decay time. d) Time-dependent effective diffusion constant after 3.14eV photoexcitation. a-d) Adapted and reproduced with permission.[42] Copyright 2016, American Association for the Advancement of Science.

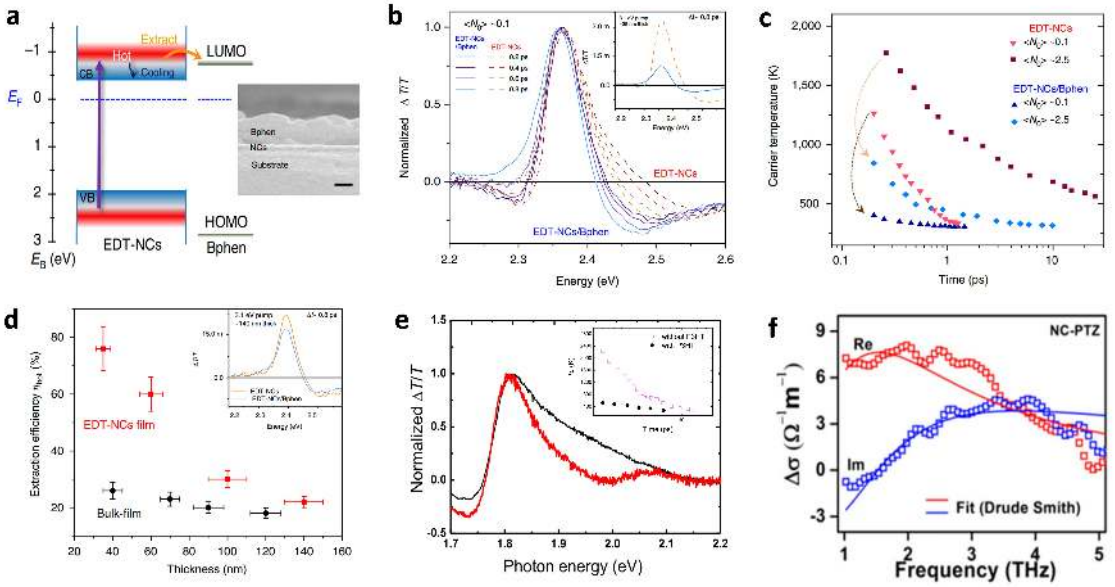

Figure 10. HC extraction from perovskites. a) Energy level diagram of perovskites NCs with Bphen (left). Cross-sectional SEM image of NCs covered with Bphen (right). Scale bar, 100 nm. b) TA spectra (normalized) of NCs film with (solid lines) and without (dashed lines) Bphen after 3.1-eV photoexcitation with a pump fluence of $\langle N_0 \rangle$ ~0.1. Inset shows the unnormalized TA spectra at a delay time of 0.8 ps. c) HC temperature versus delay time at different pump fluence. d) Film thickness dependence of HC extraction efficiencies. a-d) Reproduced with permission.[9] Copyright 2017, Nature Publishing Group. e) TA spectra of the $CsPbI_3$ film with (red) and without (black) P3HT at 0.3ps after 470 nm photoexcitation at pump fluence of 1.3 $\times 10^{18}$ cm^{-3}. Inset: extracted HC temperature versus delay time for a $CsPbI_3$ film with and without P3HT at excitation condition). e) Reproduced with permission.[38] Copyright 2018, Elsevier. f) Thz conductivity spectra for $CsPbBr_3$ NCs with PTZ under 400 nm photoexcitation, with a pump fluence of $\langle N_0 \rangle$ ~1.3. f) Reproduced with permission.[123] Copyright 2017, American Chemical Society.

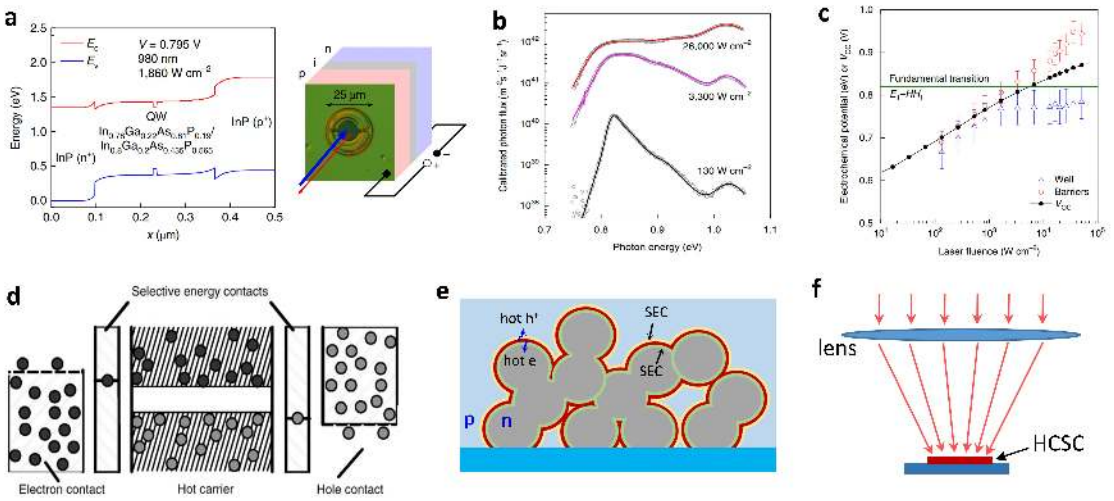

Figure 11. HCSC device implementation. a) Energy band diagram (left panel) of a III-V hot carrier heterojunction device under 980 nm laser photoexcitation and open-circuit conditions. An optical microscope image of the micro-solar cell (top-view, golden green) along with the schematic optoelectrical characterization (right panel). b) PL spectra at different laser pump fluence (grey circles) and their fits (solid lines), in the open-circuit regime. c) Variation of electrochemical potentials in the QW (red circles) and barriers (blue triangles) with laser pump fluence. a-c) Reproduced with permission.[129] Copyright 2018, Nature Publishing Group. d) A conceptual design for HCSC with energy selective contacts. Reproduced with permission. Copyright 2008, Elsevier.[130] e) Schematic illustration of separation of hot-carriers in HCSC with extremely thin absorber (ETA) layer (red layer). f) Schematic concept of concentrator perovskite HCSC.

Table 1. List of the time delays from initial HC temperature cooled to 600 K with the initially generated carrier densities and the excess energies above the band-edges in different materials.

Materials	Excess energy (eV)	Low pump fluence ($<10^{18}$cm^{-3})			High pump fluence ($>10^{18}$cm^{-3})			Technique and temporal resolution	Refs
		carrier density ($\times10^{17}$cm^{-3})	initial carrier temperature (K)	delay time to 600 K (ps)	carrier density ($\times10^{18}$ cm^{-3})	initial carrier temperature (K)	delay time to 600 K (ps)		
CdSe nanorods (solution)	~ 1.1	~5.5	~1400	~ 0.8	~22	~1400	~ 3	TRPL (~300 fs)	Achermann *et al.*[53]
GaAs film	~1.7	-	-	-	~6.0	~4000	~2	TA (~150 fs)	Y. Yang *et al.*[22]
CdS microplate	~0.65	~3.2	~900	0.4	~1.4	~900	~0.6	TRPL (~170 fs)	Klimov *et al.*[54]
InN film	~2.4	-	-	-	~3.2	-	~10	TA (~300 fs)	Fen *et al.*[51]
$MAPbI_3$ films	~1.5	~5.2	~1500	~0.6	~6.0	~4000	~60	TA (~ 150 fs)	Y. Yang *et al.*[22]
					~1.5	~2200	~10		
	~0.83	~5.2	~900	~0.3	-	-	-		
	~0.45	~5.2	~720	~0.18	-	-	-		
	~0.6	~6.4	~900	~ 0.5	~6.4	~1600	~ 1.1	TA (~200 fs)	Price *et al.*[47]
	~0.8	~6.2	~530	~0.3	~10.2	~900	~0.8	TA (~150 fs)	Fu *et al.*[46]
	~1.45	-	-	-	~4.2	~1000	~0.7		
	~1.45	-	-	-	~12	~920	~2	TA (~150 fs)	J. Yang *et al.*[30]
	~1.45	~8.9	~1800	>2500				TRPL (~16 ps)	Bretschneider *et al.*[56]
$FAPbI_3$ films	~1.55	~ 4.8	~1200	~ 0.3	~4.8	~2850	~30	TA (~150 fs)	J. Yang *et al.*[30]
	~1.5				~6.0	~4000	~30	TA (~ 150 fs)	Y. Yang *et al.*[22]
$CsPbI_3$ films	~0.8	~ 7	~1500	~ 2	~7	~2700	~10	TA (~150 fs)	Shen *et al.*[38]
$FASnI_3$ films	~1.7				~6	~1650	~1000	TRPL (10 ps)	Fang *et al.*[43]

$MAPbBr_3$ microplates	~0.7	~0.7	~580[a)]	~ 200				TRPL (~20 ps)	Zhu *et al.*[31]
$MAPbBr_3$ films	~0.7	~2.1	~350	< 0.1	~15	~900	~0.8	TA (~ 150 fs)	Li *et al.*[9]
$MAPbBr_3$ NCs		~2.6	~1650	~ 0.6	~3.5	~2200	~32		
$FAPbI_3$ NCs	~1.45	~10	~1450	~1.4	~1.1	~2300	~40	TA (100-120 fs)	Papagiorgis *et al.*[57]

a) background lattice temperature subtracted.

Mingjie Li received his BSc. (2006) and MSc. (2009) degrees in Physics from Lanzhou University, China and Ph.D. (2013) degree in Physics and Applied Physics from Nanyang Technological University, Singapore. He currently is working as a research fellow supervised by Prof. Tze-Chien Sum. His research interests include ultrafast spectroscopy study of photophysics in semiconductor and perovskites nanostructures with a focus on colloidal nanocrystals; charge carrier dynamics in light harvesting, emitting or sensing devices; optical gain and lasing.

Tze-Chien Sum received his BSc. (1999), MSc. (2000) and Ph.D. (2005) degrees in Physics from the National University of Singapore. His Ph.D. is on proton beam writing and accelerator-based ion-beam spectroscopy. Upon joining Nanyang Technological University (NTU) in 2005 as a lecturer, he switched to a new field of femtosecond time-resolved spectroscopy. Tze-Chien is presently a Professor of Physics at the Division of Physics and Applied Physics, School of Physical and Mathematical Sciences (SPMS), NTU, where he leads the Femtosecond Dynamics Laboratory. He is also the Associate Chair (Research), SPMS. His current research focuses on investigating light-matter interactions; energy and charge transfer mechanisms; and probing carrier and quasi-particle dynamics in a broad range of emergent nanoscale, light harvesting, and light emitting systems. More information can be found at http://www.ntu.edu.sg/home/tzechien/spms/index.html

Halide perovskites exhibit extraordinary properties of slow hot-carrier cooling; long-range hot-carrier transport; and efficient hot-carrier extraction that are capable of unlocking disruptive high-efficiency hot-carrier photovoltaics which will overcome the Shockley-Queisser limit. Herein, we explicate the complicated photophysical mechanisms behind the novel phenomenon; assemble an engineering and developmental toolkit; and examine the challenges and opportunities in this fledging area.

Keyword: Shockley-Queisser limit, hot carriers, halide perovskite, phonon bottleneck, hot-carrier solar cell

Mingjie Li, Jianhui Fu, Qiang Xu, and Tze Chien Sum*

Slow Hot Carrier Cooling in Halide Perovskites: Prospects for Hot-Carrier Solar Cells